IMPROVING THERMO-OPTIC PROPERTIES OF SMART WINDOWS VIA COUPLING TO RADIATIVE COOLERS

Erjun Zhang[1], Yang Cao[1], Christophe Caloz[2], Maksim Skorobogatiy[1]
1) Engineering Physics, Polytechnique Montréal
2) Electrical Engineering, Polytechnique Montréal
6079 Station Centre-Ville, Montréal, Québec, H3C 3A7, Canada

ABSTRACT

In this work we first solve the radiative heat transfer problem in one dimension to perform a comparative analysis of the time averaged performance of the partially transparent radiative windows and radiative coolers. In doing so we clearly distinguish the design goals for the partially transparent windows and radiative coolers and provide optimal choice for the material parameters to realize these goals. Thus, radiative coolers are normally non-transparent in the visible, and the main goal is to design a cooler with the temperature of its dark side as low as possible relative to that of the atmosphere. For the radiative windows, however, their surfaces are necessarily partially transparent in the visible. In the cooling mode the main question is rather about the maximal visible light transmission through the window at which the temperature on the window somber side does not exceed that of the atmosphere. We then demonstrate that transmission of the visible light through smart windows can be significantly increased (by as much as a factor of 2) without additional heating of the windows via coupling of the windows to the radiative coolers using transparent cooling liquid that flows inside of the window and radiative cooler structures. We demonstrate that efficient heat exchange between radiative coolers and smart windows can be realized using small coolant velocities (sub 1mm/s for ~1m-large windows) or even using a purely passive gravitationally driven coolant flows between a hot smart window and a cold radiative cooler mounted on top of the window with only a minimal temperature differential (sub-1K) between the two. We believe that our simple models complimented with an in-depth comparative analysis of the standalone and coupled smart windows and radiative coolers can be of interest to a broad scientific community pursuing research in these disciplines.

1. INTRODUCTION

Currently, the problem of energy overconsumption presents one of the major challenges for many societies [1]. In particular, energy spending for building cooling, heating and lighting accounts for ~40% of the total energy consumption in some countries [1,2]. While several methods to reduce energy use for the cooling of buildings, automobiles, food depots and other structures are known, radiative cooling distinguishes itself by being one of the few temperature reduction methods that require no external energy sources for their operation [1,2]. Design of radiative coolers presents an intriguing multidisciplinary problem at the intersection of physics, material science, optics and engineering.

Similarly to other cooling methods, general idea of the radiative cooling is to achieve larger energy outgoing flux than the incoming energy flux [3]. Standard passive cooling devices use large heat sinks with lower temperature than that of a cooled object to reach large outgoing energy fluxes [4]. On a planetary scale,

Corresponding author: Maksim Skorobogatiy - maksim.skorobogatiy@polymtl.ca

the Earth temperature is ~300K, which is much larger than the temperature of the outer space ~3 K that acts as an infinite heat sink for the planet [3]. As the outer space is a near perfect vacuum, the main heat loss mechanism for the Earth is not a conduction driven heat transfer but a radiative one. This is due to the fact that objects with temperatures above the absolute zero radiate electromagnetic energy known as thermal radiation or black-body radiation with the spectrum depending on the object temperature and described by the Planck's law. Thus, objects with temperatures of ~300 K mainly radiate energy in the mid-IR with a broad peak in the spectral density covering the wavelength of 8-15 μm [4]. Remarkably, in the same spectral rage, the Earth's atmosphere has a transmission window (window of transparency) that allows a considerable portion of the mid-IR thermal radiation to leave unimpeded [4,5]. This represents the main mechanism by which terrestrial objects can dissipate heat into the outer space in the form of electromagnetic waves, which is the basis of radiative cooling. It is pertinent to mention at this point that the Earth cooling via radiative heat transfer to the outer space is compensated by heating of the Earth surface via partial absorption of the radiative energy of the Sun that features the highest spectral density in the visible, while extending all the way to the near-IR 0.3-2.5 μm [6].

The study of radiative cooling has a long history. It has been well known since the ancient times that using blackened surfaces (radiators) facing a clear night sky could result in sub-ambient temperatures of the radiator, which was even used to make ice [7]. Temperature reduction of about 5°C was reported by Granqvist in 1981 [8], using a low emittance window surface and night time cooling. This original work was followed by several studies of radiative cooling efficiency under different environmental conditions, such as humidity [9,10], ambient temperature [11], and geographical location [12]. This original work was followed by studies of the day time cooling, which turned to be a much harder problem. Originally, daytime radiative cooling under direct sunlight was achieved by using a radiator that would reflect most of the sunlight, while radiating efficiently in the mid-IR spectral range [13], thus allowing the heat to escape through the atmospheric transparency window. The fact that the radiative energy of the Sun and the thermal radiation of a terrestrial object occupy different and mostly non-overlapping parts of the electromagnetic spectrum make the problem of the radiative cooler design more complicated. This is because the cooler materials have to exhibit widely different thermo-optic properties in the visible and mid-IR spectral ranges.

A large number of studies have been conducted to date on a subject of radiative cooler materials (electrochromic, photochromic windows and thermochromic windows [14-16], photonic crystals and metamaterials [13,17]), as well as structures and design optimization (reflecting vs. absorbing structures [17-19]), with experimentally demonstrated temperature reduction from 5°C to 42°C [4,13,20]. Furthermore, the question of the fundamental limit in the temperature reduction for radiative coolers was investigated in great details with a consensus that it depends strongly on the environmental conditions [10,21]. Thus, for the night time radiative coolers the predictions range between 15-42°C [21-23], while for the daytime radiative coolers the temperature reduction is expected to be only several degrees [13].

An important issue when characterizing radiating coolers is the choice of parameters to characterize the cooler performance. While the cooler itself has a working surface, its main function is to cool the air and solid objects behind it. Therefore, while the cooler surface temperature is of importance the more practical parameter is probably the air temperature or the temperature of a solid behind the cooler. Another issue is about on-average versus instantaneous performance of a cooler. While some coolers work mostly during night-time, others are capable of the day and night operation [24]. They are known as high efficiency radiative coolers or radiative windows if the cooler surface is partially transparent. Additionally, if the window can adjust its radiative properties in response to the changing environmental conditions such as ambient temperature and daylight illumination [25-27], or if it is capable of both cooling and heating, such windows are frequently referred to as intelligent or smart window [28].

Recently, there has been a strong interest in passive and active smart windows that could operate year-long, while providing heating in the cold and cooling in the hot weathers [24,29]. Much research is focusing on developing materials that can simultaneously, while independently manage radiation across several widely

spaced spectral ranges covering, for example, visible / near-IR light [12,30,31], or solar / mid-IR light [20]. At the same time, a concept of perfect smart window was proposed to judge the energy efficiency of the existing smart windows [32,33]. Thus, the perfect smart window has zero absorptivity for the visible light, near infrared and mid infrared. At the same time, the window features a perfect transmittance in the visible, while the mid-IR light transmittance and reflectance should be either (zero, perfect) or (perfect, zero) depending on whether heating or cooling is required. In any case, to switch between the heating and cooling states the intelligent windows should allow large difference in its transmittance/reflectance properties between the two states, while always featuring low absorption of solar radiation [32]. Therefore, much attention was payed to improving the performances of the smart windows through materials research and structural optimization [29,34-39].

Currently, there three main types of smart windows in development that use electrochromic, thermochromic, photochromic materials and combinations of thereof. Electrochromic materials employ reversible redox reaction that affects material's electronic transitions, and, as a consequence, the absorption profile of the solar spectra [28]. Several metal oxides have been reported for applications in smart windows among which the tungsten oxide (WO3) being the most popular one due to material's fast switching time between opaque and clear sates, as well as high visible light transmission in the clear state [40,41]. Thermochromic smart windows employ materials that exhibit phase transition between the semiconducting monoclinic phase (clear state) and the metallic rutile phase (opaque state) as a function of temperature. Vanadium dioxide (VO2) based materials are the most popular ones to regulate transmission of the visible and near-IR light using the thermochromic effect [41]. At the same time, even in the clear state transmittance of the visible light through this material is relatively low because of the material strong absorption and reflection in short wavelength range [40]. In addition, the VO2 phase transition temperature ~68 ℃ is relatively high for the practical applications, while transitions temperatures in the 20℃~30℃ would be more desired. Finally, photochromic smart window can alter its light transmission properties depending on the intensity of the incident sunlight. Photochromic materials have large working temperature range (from 20℃ to as high as 80℃), and are relatively abundant [40,42].

While much work has been done on theoretical understanding of the functioning of radiative coolers, in the related field of smart windows the performance targets and optimization strategies are still less understood. As functioning of the smart windows is dominated by the multi-year-long time scale, therefore it is interesting to analyze their averaged-over-time performance rather than an instantaneous response. It is also important to acknowledge that the function of a window implies nonzero visible light transmission, therefore a tradeoff between the window performance and its esthetic function seems unavoidable. In this respect it is interesting to investigate the possibility of improving thermo-optical performance of the smart windows by their coupling to the radiative coolers, which to our knowledge has not been studied yet.

In this paper we, therefore, consider in more details partially transparent radiative coolers in the context of their application in smart windows. From the onset we distinguish the design goals for the radiative coolers from those of the partially transparent (in the visible) radiative windows. Thus, radiative coolers are normally non-transparent in the visible, and the main goal is to design a cooler with the temperature of its dark side as low as possible compared to that of the atmosphere. For the radiative windows, however, their surfaces are necessarily partially transparent in the visible. In the cooling mode, therefore, the main question is about the maximal visible light transmission through the window at which the temperature on the window somber side does not exceed that of the atmosphere. Alternatively, as a measure of the window performance one can use the temperature of the adjacent inner air region or even that of the room wall. Finally, by coupling radiative window to the radiative cooler using active or passive heat exchange mechanisms (for example, gravitationally driven coolant flow), one can increase transmission of the visible light through the window, while maintaining the same window temperature.

In order to model precisely the smart window performance, one has to have a realistic model of the atmospheric optical properties [43], and then solve a full radiative heat transfer problem [44] that includes

atmosphere, window and enclosure where the window is installed. While certainly possible, such an overwhelming approach will most probably obscure the relatively simple physics behind the problem. Therefore, in this work we strip the radiative heat transfer problem to a bare minimum and confine ourselves to one dimension, while still retaining all the key elements of a problem. Particularly, we consider the atmosphere, the window, the cooler, and the backwall that are all in the thermal equilibrium and that all exchange the energy via radiative heat transfer, convection or coolant flow. Moreover, we use a simplified two-state model for the optical properties of an atmosphere and a window material that assumes two distinct sets of the optical reflection/absorption/transmission parameters in the visible/near-IR and mid-IR spectral ranges. Furthermore, we assume constant temperature across the radiative window/cooler, which is justified for materials with relatively high thermal conductivity. Finally, heat exchange between the window and a radiative cooler is modeled via fixed volumetric rate coolant flow between the internal elements of their structure. We believe that our work captures all the important aspects of the radiative heat transfer in smart windows and allows to make valuable qualitative predictions on the choice of the windows optimal design parameters without resorting to solution of the overcomplicated full radiative transfer problem.

2. SINGLE LAYER MODEL OF THE ATMOSPHERE

We start with a single layer model of the atmosphere [45] (see Fig. 1). This model allows to relate together the Earth and the atmosphere average temperatures (T_g and T_a), the atmosphere average emissivity $\varepsilon_a(\nu)$, the planet albedo al (reflectivity) and the total incoming radiative flux from the Sun $P(\nu)$. This model is a necessary point of departure that allows to define a self-consistent reference (average atmospheric properties versus average Sun radiative flux) for the following models of smart windows.

The model assumes equilibrium temperature distribution, and, hence, net zero radiative heat flux through any interface parallel to the Earth. A key element of the model is a recognition that in equilibrium, material absorption coefficient equals to the material emission coefficient. Namely, $\varepsilon_a(\nu)$ - the emissivity of the atmosphere at frequency ν equals to its absorption $a_a(\nu)$ as $\varepsilon_a(\nu) = a_a(\nu) = 1 - r_a(\nu) - t_a(\nu)$. Here, $r_a(\nu)$ is frequency dependent reflection coefficient of the atmosphere by power (mostly due to Rayleigh scattering), $t_a(\nu)$ is the frequency dependent transmission coefficient of the atmosphere by power given by $t_a(\nu) \approx (1 - r_a(\nu))\exp(-\alpha_a(\nu)L_a)$, where the thickness of the atmosphere is L_a and material absorption coefficient of the atmosphere by power is $\alpha_a(\nu)$. Finally, we assume that emissivity of the Earth at any frequency is 1 (blackbody approximation) and define emission spectrum (by power) of a blackbody at temperature T as $E(\nu, T)$.

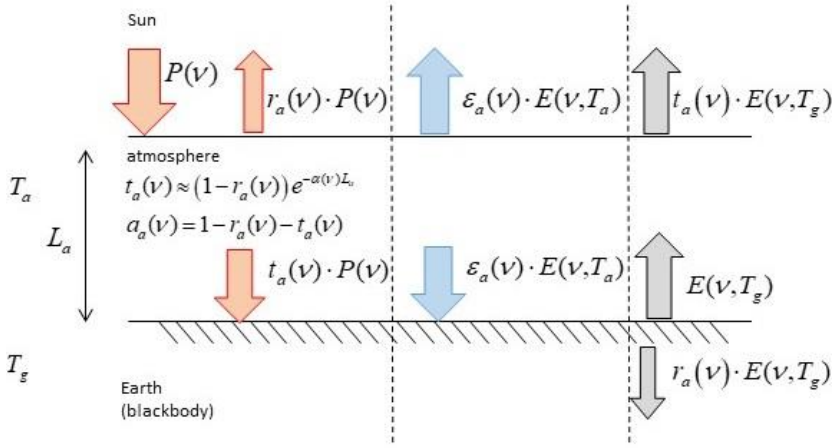

Fig. 1. Single layer model of the atmosphere

Assuming a constant temperature in the atmosphere T_a, we now use the energy conservation principle to write the following equations. At the space edge of the atmosphere we write for the energy fluxes in equilibrium:

$$\int (1-r_a(\nu))\cdot P(\nu)\, d\nu = \int \varepsilon_a(\nu)\cdot E(\nu,T_a)\, d\nu + \int t_a(\nu)\cdot E(\nu,T_g)\, d\nu \quad (1)$$

At the Earth level we write for the energy fluxes in equilibrium:

$$\int t_a(\nu)\cdot P(\nu)\, d\nu = -\int \varepsilon_a(\nu)\cdot E(\nu,T_a)\, d\nu + \int (1-r_a(\nu))\cdot E(\nu,T_g)\, d\nu \quad (2)$$

Alternatively, by subtracting (2) from (1) we also get the balance between the absorbed and irradiated energy in the atmosphere:

$$2\int \varepsilon_a(\nu)\cdot E(\nu,T_a)\, d\nu = \int a_a(\nu)\cdot P(\nu)\, d\nu + \int a_a(\nu)\cdot E(\nu,T_g)\, d\nu \quad (3)$$

Now, we introduce several approximations for the values of the various parameters involved in the model (1)-(3) using physical properties of the atmosphere.

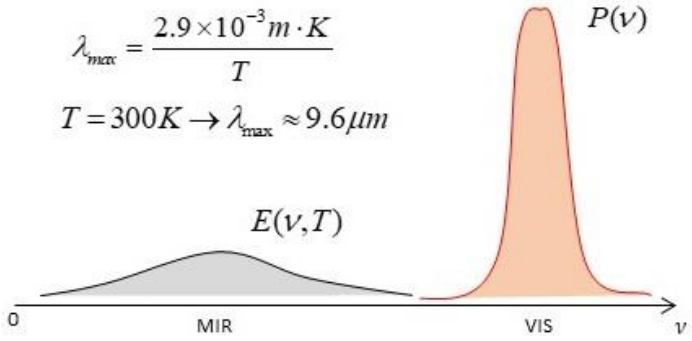

Fig. 2. Power of the incoming light is mostly concentrated in the visible spectral range, while power of the irradiated light by the atmosphere and Earth are mostly in the Mid-IR spectral range.

First, we note that power of the incoming light from the Sun is mostly concentrated in the visible spectral range, while power of the irradiated light by the atmosphere and Earth are mostly in the mid-IR spectral range, with little overlap between the two (see Fig. 2). Therefore, instead of using frequency-variable transmission and reflection properties of the atmosphere, we rather assume a step-like spectral behavior of its optical properties. Particularly, we assume that in the visible and in the mid-IR spectral ranges, the optical properties of the atmosphere are distinct from each other and frequency invariable as shown in Fig. 3.

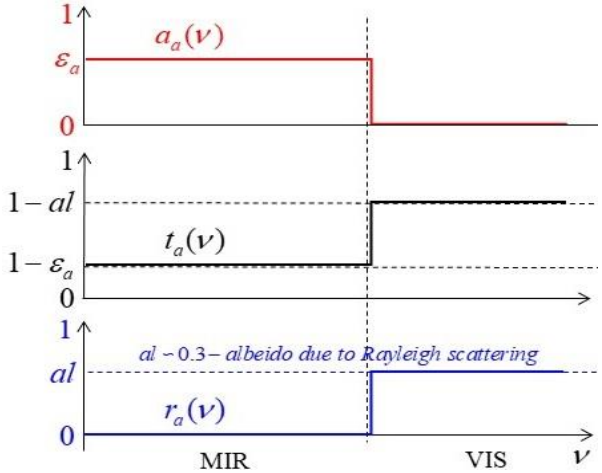

Fig. 3. Step-like model for the frequency dependent optical properties of the atmosphere (absorption, transmission and reflection).

With thus defined properties of the atmosphere we get the following values for the various integrals:

$$\int t_a(\nu)\cdot P(\nu)d\nu = (1-al)\int P(\nu)d\nu = (1-al)\,\bar{P} \quad ; \quad \int (1-r_a(\nu))\cdot P(\nu)d\nu = (1-al)\,\bar{P}$$
$$\int (1-r_a(\nu))\cdot E(\nu,T_g)d\nu = \sigma T_g^4 \quad ; \quad \int t_a(\nu)\cdot E(\nu,T_g)d\nu = (1-\varepsilon_a)\,\sigma T_g^4 \qquad (4)$$
$$\int \varepsilon_a(\nu)\cdot E(\nu,T_a)d\nu = \varepsilon_a \sigma T_a^4 \quad ; \quad \int a_a(\nu)\cdot P(\nu)d\nu = 0 \quad ; \quad \int a_a(\nu)\cdot E(\nu,T_g)d\nu = \varepsilon_a \sigma T_g^4$$

while equations (1), (2) and (3) (only two of the three are independent) become:

$$\begin{cases} (1-al)\,\bar{P} = \varepsilon_a \sigma T_a^4 + (1-\varepsilon_a)\,\sigma T_g^4 \\ (1-al)\,\bar{P} = -\varepsilon_a \sigma T_a^4 + \sigma T_g^4 \\ 2\cdot T_a^4 = T_g^4 \end{cases} \qquad (5)$$

from which is follows that:

$$\sigma T_a^4 = \frac{(1-al)}{(2-\varepsilon_a)}\,\bar{P} \qquad (6)$$
$$T_g = 2^{1/4}\cdot T_a$$

In order to reproduce with this model the average Earth temperature $T_g = 288.2$, while using for the planet albedo $al = 0.3$, and the average radiative flux from the Sun incident onto the planet $\bar{P} = 342 W\cdot m^{-2}$, one requires to choose for the atmosphere emissivity $\varepsilon_a = 0.78$. This also results in a somewhat low atmospheric temperature $T_a = 242.11K$ ($-30^{\circ}C$), which is a well know deficiency of a single layer atmospheric model. Note that the quoted value for the average incoming solar radiation takes into account the angle at which the rays strike and that at any one moment half the planet does not receive any solar radiation. It therefore measures only one-fourth of the solar constant, which is an averaged over the year energy flux incident on the Earth as measured by an orbiting satellite.

3. SINGLE LAYER, PARTIALLY TRANSPARENT RADIATIVE WINDOW

We now consider a single layer optically symmetric window placed in the path of a sunlight (see Fig. 5). The window is assumed to be optically thick (no interference effects). We also assume that the temperature across the window is constant and equal to T_w, and, therefore, the thermal radiation from the window is the same in both directions. Validity of this approximation is studied in the Supplementary Material A, where we solve a full radiative heat transfer model for a standalone slab and show that temperature inside can be considered constant if the slab is made of material with high enough thermal conductivity. Behind the window we place a perfect absorber that we refer to as a wall, and temperature of the wall surface behind the window, which is considered to be a blackbody, represented by T_s. The wall is assumed to be thermally and radiationally separated from the ground. We, furthermore, assume that there is vacuum between the window and the wall, so we neglect the convection and conduction heat transfer in this region. Finally, the Earth atmosphere is characterized by the average temperature and permittivity defined in the previous section.

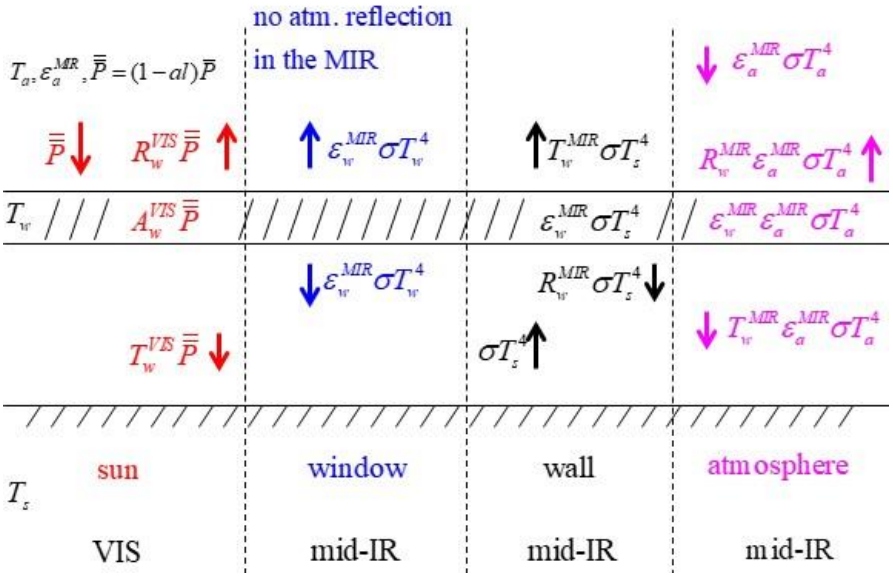

Fig. 5. Model of the optically symmetric single layer window (no convection/conduction between the wall and the window).

Spectral dependence of the window material parameters ($r_w(\nu)$, $t_w(\nu)$, $a_w(\nu)$) are assumed to be step-like, with two distinct sets of frequency independent parameters defining window properties in the mid-IR and visible ranges as shown in Fig. 4.

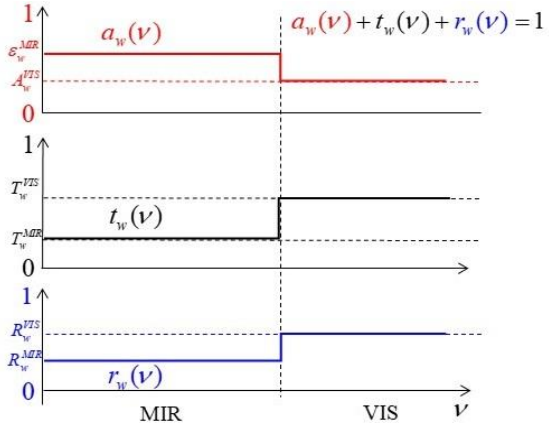

Fig. 4. Step-like model for the frequency dependent optical properties of the window (absorption, transmission and reflection).

Spectrum of the incoming radiation from the sun at the ground level by power is given by $P_g(\nu) = t_a(\nu) \cdot P(\nu)$, and average power of the sun at the planet (window) surface is given by $\bar{\bar{P}} = (1-al)\bar{P}$.

We now use the energy conservation principle to write the following equations. At the window / atmosphere interface we write for the energy fluxes in equilibrium:

$$\int (1-r_w(\nu)) \cdot P_g(\nu)\, d\nu = \int \varepsilon_w(\nu) \cdot E(\nu, T_w)\, d\nu + \int t_w(\nu) \cdot E(\nu, T_s)\, d\nu - \int \left(1-r_w(\nu)\right) \cdot \varepsilon_a(\nu) \cdot E(\nu, T_a)\, d\nu \quad (7)$$

At the wall (blackbody) level we write for the energy fluxes in equilibrium:

$$\int t_w(\nu) \cdot P_g(\nu)\, d\nu = -\int \varepsilon_w(\nu) \cdot E(\nu, T_w)\, d\nu + \int (1-r_w(\nu)) \cdot E(\nu, T_s)\, d\nu - \int t_w(\nu) \cdot \varepsilon_a(\nu) \cdot E(\nu, T_a)\, d\nu \quad (8)$$

Alternatively, by subtracting (8) from (7) we also get the balance between the absorbed and irradiated energy in the window:

$$2\int \varepsilon_w(\nu) \cdot E(\nu, T_w)\, d\nu = \int a_w(\nu) \cdot P(\nu)\, d\nu + \int a_w(\nu) \cdot E(\nu, T_s)\, d\nu + \int a_w(\nu) \cdot \varepsilon_a(\nu) \cdot E(\nu, T_a)\, d\nu \quad (9)$$

These equations can be further simplified when using a step-like model for the material optical properties (only two of the three following equation are independent):

$$\begin{cases} (1-R_w^{VIS})\cdot\bar{\bar{P}} = \varepsilon_w^{MIR}\cdot\sigma T_w^4 + T_w^{MIR}\cdot\sigma T_s^4 - (1-R_w^{MIR})\cdot\varepsilon_a\sigma T_a^4 \\ T_w^{VIS}\cdot\bar{\bar{P}} = -\varepsilon_w^{MIR}\cdot\sigma T_w^4 + (1-R_w^{MIR})\cdot\sigma T_s^4 - T_w^{MIR}\cdot\varepsilon_a\sigma T_a^4 \\ 2\varepsilon_w^{MIR}\cdot\sigma T_w^4 = A_w^{VIS}\cdot\bar{\bar{P}} + \varepsilon_w^{MIR}\cdot\sigma T_s^4 + \varepsilon_w^{MIR}\cdot\varepsilon_a\sigma T_a^4 \end{cases} \quad (10)$$

Now, using (10), as well as results of the model 1 that relates average atmospheric temperature to the average power flux arriving at the planet surface, we can arrive to the following expressions for the temperatures of the window and the wall:

$$\frac{T_w^4}{T_a^4} = \varepsilon_a + \left(2-\varepsilon_a\right)\frac{T_w^{VIS} + A_w^{VIS}\cdot\left(1+\frac{T_w^{MIR}}{\varepsilon_w^{MIR}}\right)}{2T_w^{MIR}+\varepsilon_w^{MIR}}$$

$$\frac{T_s^4}{T_a^4} = \varepsilon_a + \left(2-\varepsilon_a\right)\frac{2T_w^{VIS} + A_w^{VIS}}{2T_w^{MIR}+\varepsilon_w^{MIR}} \quad (11)$$

The radiative heat transfer model for a single layer partially transparent window can be readily extended to account for the convection heat transfer between the window and the air that surrounds it. The resultant model is virtually identical to the one presented in this section and includes only two new parameters, which are the room temperature (in the space between the window and the wall), and the heat transfer coefficient h. For completeness, we detail this model and its analysis in Supplementary Material B. The key conclusion derived from analysis of this model is that convection heat transfer always reduces efficiency of the radiative coolers and windows more so for stronger convection rates. Convection contribution becomes important for large enough values of the heat transfer coefficient $h/\left(8\sigma T_a^3\right) > (2T_w^{MIR}+\varepsilon_w^{MIR})$, which is equivalent to $h > 6.46[W/K]\cdot(2T_w^{MIR}+\varepsilon_w^{MIR})$ when operating in the vicinity of standard ambient temperatures. The value of the heat transfer coefficient depends strongly on the temperature differential, as well as the window size and orientation and is generally in the $1-10[W/K]$ range (see Supplementary Material C for more details).

3.1 Analysis of the thermal properties of a single layer radiative window

Here we present performance analysis of various radiative windows as predicted by the model presented in the previous section. Particularly, we study the trade-off between transmission of the visible light through the radiative window and its temperature, as well as the wall temperature behind the window.

1) A particular solutions of this model (Eq. 11) is $T_w = T_s = T_a$ when choosing $T_w^{VIS} = \gamma\cdot T_w^{MIR}$, $A_w^{VIS} = \gamma\cdot\varepsilon_w^{MIR}$, for any values of $T_w^{MIR}, \varepsilon_w^{MIR}$, where $\gamma = \frac{1-\varepsilon_a}{2-\varepsilon_a} = 0.18$. Particularly, in the case of highly transmissive windows in the mid-IR $T_w^{MIR}\to 1$, which simultaneously feature low absorption in the visible $A_w^{VIS} = \gamma\cdot\varepsilon_w^{MIR} = \gamma\cdot\left(1-T_w^{MIR}-R_w^{MIR}\right)\to 0$, window transmission of the visible light can be as high as $T_w^{VIS} = \gamma = 18\%$, while both the room and the wall temperature will not exceed that of the atmosphere.

2) If the window is an efficient absorber or reflector, so that there is no transmission through the window both in the visible and in the mid-IR $T_w^{VIS} = T_w^{MIR} = 0$, then:

$$\frac{T_s^4}{T_a^4} = \frac{T_w^4}{T_a^4} = \varepsilon_a + \left(2-\varepsilon_a\right)\frac{A_w^{VIS}}{\varepsilon_w^{MIR}} \quad (12)$$

Particularly, if the window absorption in the visible is much smaller that the window absorption in the mid-IR, then the window is an efficient radiative cooler with the window and wall temperatures smaller than that of an atmosphere:

$$A_w^{VIS} \ll \varepsilon_w^{MIR} \Rightarrow T_s = T_w \approx \varepsilon_a^{1/4} \cdot T_a \approx 0.94 \cdot T_a$$

Alternatively, if the window is a black body or a "balanced" vis/mid-IR absorber, then the window and wall temperature will be those of a ground:

$$A_w^{VIS} = \varepsilon_w^{MIR} \Rightarrow T_s = T_w = 2^{1/4} T_a = T_g$$

Finally, if the window is a strong absorber in the visible, but a week absorber in the mid-IR, it becomes an efficient radiative heater:

$$A_w^{VIS} > \varepsilon_w^{MIR} \Rightarrow T_s = T_w > T_g$$

3) What is the smallest wall temperature T_s possible? From (11) it follows that:

$$\begin{aligned} &\min\left(T_s\right) = \varepsilon_a^{1/4} \cdot T_a \approx 0.94 \cdot T_a \\ &\text{when } \frac{2T_w^{VIS} + A_w^{VIS}}{2T_w^{MIR} + \varepsilon_w^{MIR}} = 0 \\ &\Rightarrow T_w^{VIS} \to 0 \; ; \; A_w^{VIS} \to 0 \Rightarrow R_w^{VIS} \to 1 \\ &\text{we must also require } 2T_w^{MIR} + \varepsilon_w^{MIR} = 1 + T_w^{MIR} - R_w^{MIR} \neq 0 \Rightarrow R_w^{MIR} \neq 1 \end{aligned} \tag{13}$$

This is the case of an almost completely reflective window in the visible, which at the same time has a non-perfect reflectivity in the mid-IR.

4) What is the smallest window temperature T_w possible? From (11) it follows that:

$$\begin{aligned} &\min\left(T_w\right) = \varepsilon_a^{1/4} \cdot T_a \approx 0.94 \cdot T_a \\ &\text{when } \frac{T_w^{VIS} + A_w^{VIS} \cdot \left(1 + \dfrac{T_w^{MIR}}{\varepsilon_w^{MIR}}\right)}{2T_w^{MIR} + \varepsilon_w^{MIR}} = 0 \Rightarrow T_w^{VIS} \to 0 \; ; \; A_w^{VIS} \to 0 \; ; \; \frac{A_w^{VIS}}{\varepsilon_w^{MIR}} \to 0 \\ &\Rightarrow R_w^{VIS} \to 1 \; ; \; A_w^{VIS} \ll \varepsilon_w^{MIR} \\ &\text{we must also require } 2T_w^{MIR} + \varepsilon_w^{MIR} = 1 + T_w^{MIR} - R_w^{MIR} \neq 0 \Rightarrow R_w^{MIR} \neq 1 \end{aligned} \tag{14}$$

This is the case of an almost completely reflective window in the visible, which at the same time has a non-perfect reflectivity in the mid-IR. Additionally we have to require that the window absorption in the visible should be much smaller than the window absorption in the mid-IR.

5) What is the maximal transmission of the visible light through the window T_w^{VIS}, so that the wall temperature does not exceed the atmospheric temperature $T_s < T_a$? From (11) it follows that:

$$\begin{aligned} &\frac{T_s^4}{T_a^4} = \varepsilon_a + \left(2 - \varepsilon_a\right) \frac{2T_w^{VIS} + A_w^{VIS}}{2T_w^{MIR} + \varepsilon_w^{MIR}} < 1 \\ &T_w^{VIS} < \frac{1}{2} \frac{1 - \varepsilon_a}{2 - \varepsilon_a} \left(1 + T_w^{MIR} - R_w^{MIR}\right) - \frac{A_w^{VIS}}{2} \\ &\max\left(T_w^{VIS}\right) = \gamma \text{ when } T_w^{MIR} = 1 \; (\varepsilon_w^{MIR} = R_w^{MIR} = 0) \; ; \; A_w^{VIS} = 0 \\ &\text{where } \gamma = \frac{1 - \varepsilon_a}{2 - \varepsilon_a} = 0.18 \end{aligned} \tag{15}$$

In order to achieve maximal transmission of the visible light, while still having the wall temperature below that of the atmosphere, we have to demand that window absorption in the visible is zero $A_w^{VIS} \to 0$, while window transmission in the mid-IR is almost perfect $T_w^{MIR} \to 1$.

6) What is the maximal transmission of the visible light through the window T_w^{VIS}, so that the window temperature does not exceed the atmospheric temperature $T_w < T_a$? From (11) it follows that:

$$\frac{T_w^4}{T_a^4} = \varepsilon_a + \left(2-\varepsilon_a\right)\frac{T_w^{VIS} + A_w^{VIS}\cdot\left(1+\dfrac{T_w^{MIR}}{\varepsilon_w^{MIR}}\right)}{2T_w^{MIR}+\varepsilon_w^{MIR}} < 1$$

$$T_w^{VIS} < \frac{1-\varepsilon_a}{2-\varepsilon_a}\left(1+T_w^{MIR}-R_w^{MIR}\right) - A_w^{VIS}\cdot\left(1+\frac{T_w^{MIR}}{\varepsilon_w^{MIR}}\right) \qquad (16)$$

$$\max\left(T_w^{VIS}\right) = 2\gamma = 0.36 \text{ when } T_w^{MIR} \to 1\ (\varepsilon_w^{MIR}, R_w^{MIR} \to 0)\ ;\ A_w^{VIS} \ll \varepsilon_w^{MIR} \to 0$$

In order to achieve maximal transmission of the visible light, while still having the window temperature below that of the atmosphere, we have to demand that window transmission in the mid-IR is almost perfect $T_w^{MIR} \to 1$, while window absorption in the visible is much smaller than that in the mid-IR, and at the same time approaching zero $A_w^{VIS} \to 0$.

7) Tradeoff between window transmission and absorption in the visible can be summarized geometrically in Fig. 6. As follows from inequalities (15) and (16), shaded regions below the corresponding lines represent the range of values of T_w^{VIS}, A_w^{VIS} for which either the wall temperature or the window temperature are smaller than the atmospheric temperature. Intersection of these two regions represent the range of values of T_w^{VIS}, A_w^{VIS} for which both the wall temperature and the window temperature are smaller than the atmospheric one. Both the window and the wall temperatures attain that of the atmospheric one when $T_w^{VIS} = \gamma \cdot T_w^{MIR}$, $A_w^{VIS} = \gamma \cdot \varepsilon_w^{MIR}$. As clear from the graph, when $T_w^{VIS} \le \gamma \cdot T_w^{MIR}$ and $A_w^{VIS} \le \gamma \cdot \varepsilon_w^{MIR}$, it is guaranteed that both the window and the wall temperatures will be smaller than the atmospheric temperature.

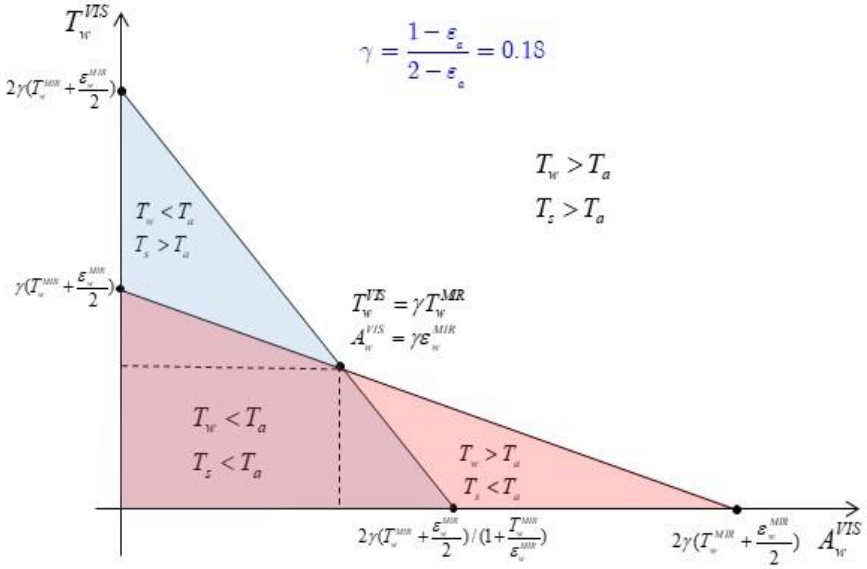

Fig. 6. Tradeoff between window transmission and absorption in the visible (no convection). A region of parameter space that is situated below the two lines define window operation regime for which both the wall and the window temperatures are smaller than that of the atmosphere.

4. PARTIALLY TRANSPARENT SMART WINDOW THAT IS THERMALLY COUPLED TO A RADIATIVE COOLER

An idea that we explore in this section is to exploit the cooling properties of passive radiative coolers in order to enhance transmission of the visible light through the smart windows, without increasing the window temperature or the temperature of the wall behind it. This idea can be of practical significance as there were recent reports of successful cooling of water (coolant) flowing through the internal structure of a radiative cooler [48]. Particularly, we envision a transparent (in the visible) coolant that passively or actively flows through the window and the radiative cooler inner structures (see Fig. 7). The coolant carries the heat from the partially transparent window which is then dissipated into the atmosphere by the radiative cooler. The goal of this section is to quantify the potential improvements in the intensity of transmitted visible light through the window offered by such a hybrid structure.

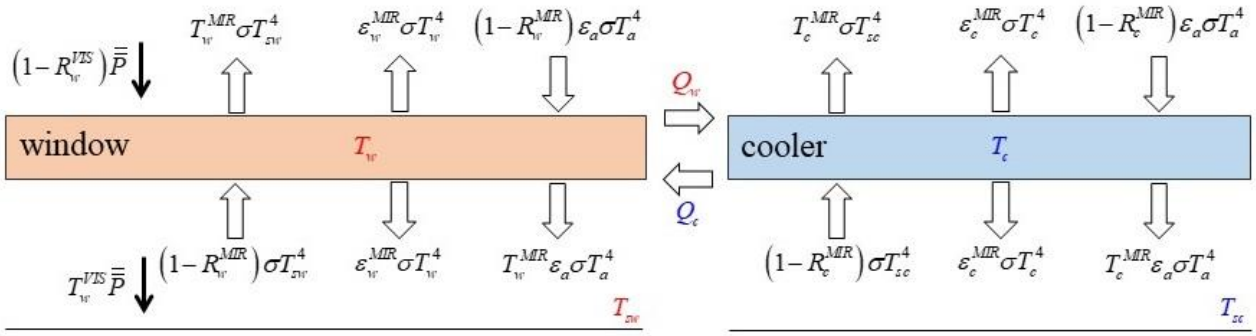

Fig. 7. Thermally coupled radiative cooler and partially transparent window via exchange of a cooling fluid. Thus cooled windows can offer higher transmission intensities of the visible light compared to a standalone window.

As established in the previous sections, there is a tradeoff between transmitted intensity of the visible light and the temperature of the widow and the backwall. For example, we have established that the maximal transmission of the visible light through the window T_w^{VIS}, so that the window temperature does not exceed the atmospheric temperature $T_w < T_a$ equals to $\max\left(T_w^{VIS}\right) = 2\gamma$, where $\gamma = \frac{1-\varepsilon_a}{2-\varepsilon_a} = 0.18$ and we have to demand that the window absorption in the visible is zero $A_w^{VIS} \to 0$, while window transmission in the mid-IR is almost perfect $T_w^{MIR} \to 1$. Additionally, we have established that in the case of radiative coolers, the cooler temperature can be made significantly smaller than that of the atmosphere $\min\left(T_w\right) = \varepsilon_a^{1/4} \cdot T_a \approx 0.94 \cdot T_a$ by requiring that the cooler surface is almost completely reflective in the visible, and that the radiative cooler absorption in the visible is much smaller than the window absorption in the mid-IR. In what follows we explore a scenario where smart window and a radiative cooler are thermally coupled. In this case, radiative cooler is used to reduce the temperature of a smart window, which, in turn, allows to increase the intensity of transmitted visible light through the window, without increasing the window temperature beyond that of the atmosphere.

Particularly, we consider two channels, one inside of a smart window and another one inside a radiative cooler that contain a transparent (in the visible coolant) fluid such as water or oil characterized by the volume heat capacity C_v. We suppose that the liquid flows in a closed loop between a smart window and a radiative cooler with a flow speed v_f, and that both channels have the same crossection area $A_{channel} \sim L \cdot d$, while both the cooler and the window have the same radiative areas $A_{rad.area} \sim L^2$, where L is a characteristic window/cooler size, and d is the coolant channel size. Then, the heat transfer rate (per unit area) from the window Q_w and the cooler Q_c can be defined as:

$$Q_w = \zeta \cdot T_w \quad ; \quad Q_c = \zeta \cdot T_c \qquad (17)$$

where the heat transfer rate per unit temperature is defined as $\zeta = C_v \cdot \frac{A_{channel}}{A_{rad.area}} \cdot v_f \left[W/\left(m^2 K\right) \right]$. Then, using energy conservation of the radiative and thermal fluxes we can get the modified system of equations that describe coupled window/radiative cooler system similar to that presented in the previous sections. Thus, using subscripts *c* to indicate cooler variables, while using subscript *w* to indicate window variables (also see Fig. 7) we write:

$$\begin{cases} A_w^{VIS} \cdot \bar{\bar{P}} + \varepsilon_w^{MIR} \cdot \sigma T_{sw}^4 + \varepsilon_w^{MIR} \cdot \varepsilon_a \sigma T_a^4 + \left(T_c - T_w\right) \cdot \zeta = 2\varepsilon_w^{MIR} \cdot \sigma T_w^4 \\ T_w^{VIS} \cdot \bar{\bar{P}} + T_w^{MIR} \cdot \varepsilon_a \sigma T_a^4 + \varepsilon_w^{MIR} \cdot \sigma T_w^4 = (1 - R_w^{MIR}) \cdot \sigma T_{sw}^4 \\ \\ A_c^{VIS} \cdot \bar{\bar{P}} + \varepsilon_c^{MIR} \cdot \sigma T_{sc}^4 + \varepsilon_c^{MIR} \cdot \varepsilon_a \sigma T_a^4 + \left(T_w - T_c\right) \cdot \zeta = 2\varepsilon_c^{MIR} \cdot \sigma T_c^4 \\ T_c^{VIS} \cdot \bar{\bar{P}} + T_c^{MIR} \cdot \varepsilon_a \sigma T_a^4 + \varepsilon_c^{MIR} \cdot \sigma T_c^4 = (1 - R_c^{MIR}) \cdot \sigma T_{sc}^4 \end{cases} \qquad (18)$$

While analytical solution of (18) is possible after linearization of the forth order temperature terms, due to large number of materials coefficients, the resultant expressions are complicated. To demonstrate how coupling of a radiative cooler to a window can result in the window enhanced transmission properties, we first consider a particular case of strongly absorbing in the mid-IR cooler and window materials $\varepsilon_w^{MIR} = \varepsilon_c^{MIR} = 1$. Moreover, for the radiative cooler we suppose that all the visible radiation is reflected without absorption $T_c^{VIS} = A_c^{VIS} = 0$. Finally, we suppose that window material does not absorb visible light $A_w^{VIS} = 0$. In this case one can demonstrate that $T_{sc} = T_c$, while equations (18) can be simplified as follows:

$$\begin{cases} \frac{T_w^4}{T_a^4} = T_w^{VIS} \cdot \frac{\bar{\bar{P}}}{\sigma T_a^4} + \varepsilon_a + \left(\frac{T_c}{T_a} - \frac{T_w}{T_a} \right) \cdot \frac{\zeta}{\sigma T_a^3} \\ \frac{T_{sw}^4}{T_a^4} = 2 \cdot T_w^{VIS} \cdot \frac{\bar{\bar{P}}}{\sigma T_a^4} + \varepsilon_a + \left(\frac{T_c}{T_a} - \frac{T_w}{T_a} \right) \cdot \frac{\zeta}{\sigma T_a^3} \\ \frac{T_c^4}{T_a^4} = \varepsilon_a + \left(\frac{T_w}{T_a} - \frac{T_c}{T_a} \right) \cdot \frac{\zeta}{\sigma T_a^4} \end{cases} \qquad (19)$$

Linearization of Eq. (20) around T_a by using $T^4 = \left(T_a + \delta T\right)^4 \approx T_a^4 + 4T_a^3 \cdot \delta T$ we can transform (19) into:

$$\begin{cases} \frac{\delta T_w}{T_a} = T_w^{VIS} \cdot \frac{\bar{\bar{P}}}{4\sigma T_a^4} - \frac{1 - \varepsilon_a}{4} + \left(\frac{\delta T_c}{T_a} - \frac{\delta T_w}{T_a} \right) \cdot \frac{\zeta}{4\sigma T_a^3} \\ \frac{\delta T_{sw}}{T_a} = T_w^{VIS} \cdot \frac{\bar{\bar{P}}}{2\sigma T_a^4} - \frac{1 - \varepsilon_a}{4} + \left(\frac{\delta T_c}{T_a} - \frac{\delta T_w}{T_a} \right) \cdot \frac{\zeta}{4\sigma T_a^3} \\ \frac{\delta T_c}{T_a} = -\frac{1 - \varepsilon_a}{4} + \left(\frac{\delta T_w}{T_a} - \frac{\delta T_c}{T_a} \right) \cdot \frac{\zeta}{4\sigma T_a^3} \end{cases} \qquad (20)$$

Finally, remembering expression for $\bar{\bar{P}} = \left(2 - \varepsilon_a\right) \cdot \sigma T_a^4$ from a single layer model of the atmosphere, equation (20) can be rewritten in the following form:

$$\begin{cases} \dfrac{\delta T_w}{T_a} = -\dfrac{1-\varepsilon_a}{4} + T_w^{VIS} \cdot \dfrac{2-\varepsilon_a}{8}\left(1+\left(1+\dfrac{\zeta}{2\sigma T_a^3}\right)^{-1}\right) \\ \dfrac{\delta T_{sw}}{T_a} = -\dfrac{1-\varepsilon_a}{4} + T_w^{VIS} \cdot \dfrac{2-\varepsilon_a}{8}\left(3+\left(1+\dfrac{\zeta}{2\sigma T_a^3}\right)^{-1}\right) \\ \dfrac{\delta T_c}{T_a} = -\dfrac{1-\varepsilon_a}{4} + T_w^{VIS} \cdot \dfrac{2-\varepsilon_a}{8}\left(1-\left(1+\dfrac{\zeta}{2\sigma T_a^3}\right)^{-1}\right) \end{cases} \quad (21)$$

Thus, in the case of no heat exchange between radiative cooler and a window $\zeta = 0$ we retrieve results of Section 2, while in the case of efficient heat exchange between the radiative cooler and a window $\zeta / 2\sigma T_a^3 >> 1$ we find that both the window and the wall (behind the window) temperatures have decreased, while the temperature of the cooler surface has increased

$$\begin{array}{l} \dfrac{\delta T_w}{T_a} = -\dfrac{1-\varepsilon_a}{4} + T_w^{VIS} \cdot \dfrac{2-\varepsilon_a}{8} \cdot 2 \\ \dfrac{\delta T_{sw}}{T_a} = -\dfrac{1-\varepsilon_a}{4} + T_w^{VIS} \cdot \dfrac{2-\varepsilon_a}{8} \cdot 4 \\ \underbrace{\dfrac{\delta T_c}{T_a} = -\dfrac{1-\varepsilon_a}{4}}_{\text{no heat exchange between window and cooler } \zeta = 0} \end{array} \rightarrow \begin{array}{l} \dfrac{\delta T_w}{T_a} = -\dfrac{1-\varepsilon_a}{4} + T_w^{VIS} \cdot \dfrac{2-\varepsilon_a}{8} \cdot 1 \\ \dfrac{\delta T_{sw}}{T_a} = -\dfrac{1-\varepsilon_a}{4} + T_w^{VIS} \cdot \dfrac{2-\varepsilon_a}{8} \cdot 3 \\ \underbrace{\dfrac{\delta T_c}{T_a} = \dfrac{\delta T_w}{T_a}}_{\text{strong heat exchange between window and cooler } \zeta \gg 2\sigma T_a^3} \end{array} \quad (22)$$

From expressions (22) it also follows that maximal visible transmission through the window can be increased in the case of a coupled radiative cooler / window system, while still maintaining the window and the wall (behind the window) temperatures below that of the atmosphere. For example, in the case of a standalone window, from (22) it follows that both the wall and the window temperatures are smaller than the atmosphere $\delta T_w, \delta T_{sw} < 0$ as long as $T_w^{VIS} < \dfrac{\gamma}{2} \approx 0.09$. At the same time, for the thermally coupled window and radiative cooler, it follows from (22) that both the wall and the window temperatures are smaller than that of the atmosphere as long as $T_w^{VIS} < \dfrac{2}{3}\gamma \approx 0.12$, which is a significant improvement over the uncoupled case.

4.1 Enhancement of the visible transmission of a smart window coupled to a radiative cooler as a function of the heat exchange efficiency between the two. General case

Finally, in the general case of nonlinear equations (18), analytical solution can still be found in the limit of strong heat exchange $\zeta / \left(4\sigma T_a^3\right) \gg \sqrt{\varepsilon_w^{MIR} \varepsilon_c^{MIR}}$ (this condition can be derived in a general case by linearizing nonlinear terms in (18)). Indeed, in that case the temperature of the window will be equal to the temperature of the radiative cooler and to that of the cooler fluid $T_w \approx T_c = T_f$ and the system equations (18) can be simplified by adding the first and the third equations to give:

$$\begin{cases} \left(A_w^{VIS} + A_c^{VIS}\right) \cdot \bar{\bar{P}} + \left(\varepsilon_w^{MIR} + \varepsilon_c^{MIR}\right) \cdot \varepsilon_a \sigma T_a^4 + \varepsilon_w^{MIR} \cdot \sigma T_{sw}^4 + \varepsilon_c^{MIR} \cdot \sigma T_{sc}^4 = 2\left(\varepsilon_w^{MIR} + \varepsilon_c^{MIR}\right) \cdot \sigma T_f^4 \\ T_w^{VIS} \cdot \bar{\bar{P}} + T_w^{MIR} \cdot \varepsilon_a \sigma T_a^4 + \varepsilon_w^{MIR} \cdot \sigma T_f^4 = (1 - R_w^{MIR}) \cdot \sigma T_{sw}^4 \\ T_c^{VIS} \cdot \bar{\bar{P}} + T_c^{MIR} \cdot \varepsilon_a \sigma T_a^4 + \varepsilon_c^{MIR} \cdot \sigma T_f^4 = (1 - R_c^{MIR}) \cdot \sigma T_{sc}^4 \end{cases} \quad (23)$$

Remembering expression for $\bar{\bar{P}} = (2-\varepsilon_a)\cdot\sigma T_a^4$ from a single layer model of the atmosphere, system of equations (23) can then be solved analytically to give:

limit of strong heat exchange $\zeta/4\sigma T_a^3 >> 1$:

$$\left.\frac{T_w^4}{T_a^4}\right|_{\zeta\to\infty} = \left.\frac{T_c^4}{T_a^4}\right|_{\zeta\to\infty} = \varepsilon_a + (2-\varepsilon_a)\cdot\frac{T_w^{VIS} + A_w^{VIS}\cdot\left(1+\frac{T_w^{MIR}}{\varepsilon_w^{MIR}}\right) + T_c^{VIS} + A_c^{VIS}\cdot\left(1+\frac{T_c^{MIR}}{\varepsilon_c^{MIR}}\right)}{2T_w^{MIR} + \varepsilon_w^{MIR} + 2T_c^{MIR} + \varepsilon_c^{MIR}} \tag{24}$$

no heat exchange $\zeta = 0$:

$$\left.\frac{T_w^4}{T_a^4}\right|_{\zeta=0} = \varepsilon_a + (2-\varepsilon_a)\frac{T_w^{VIS} + A_w^{VIS}\cdot\left(1+\frac{T_w^{MIR}}{\varepsilon_w^{MIR}}\right)}{2T_w^{MIR} + \varepsilon_w^{MIR}} \quad ; \quad \left.\frac{T_c^4}{T_a^4}\right|_{\zeta=0} = \varepsilon_a + (2-\varepsilon_a)\frac{T_c^{VIS} + A_c^{VIS}\cdot\left(1+\frac{T_c^{MIR}}{\varepsilon_c^{MIR}}\right)}{2T_c^{MIR} + \varepsilon_c^{MIR}}$$

From (24) it follows that the temperature of a smart window in the limit of strong heat exchange with a radiative cooler will always be smaller than that of a standalone window $T_w|_{\zeta\to\infty} < T_w|_{\zeta=0}$ as long as the temperature of a standalone radiative cooler is smaller than that of a standalone window $T_c|_{\zeta=0} < T_w|_{\zeta=0}$.

4.2 Potential realizations of the strong heat exchange regime between smart windows and radiative coolers

Here, we consider several practical examples of the forced and the gravitationally driven heat exchanges between a smart window and a radiative cooler of characteristic size $L \sim 1\ m$. We suppose that the heat transfer between the two is realized via exchange of a coolant that flows across the edge of the window and into the cooler (see Fig. 7). Assuming that the coolant fluid of volumetric heat capacity $C_v \sim 4\cdot 10^6\ \ J/(m^3 K)$ (water) flows through a channel of size $d \sim 3\ mm$ (and width $\sim L$), then the coolant flow speed necessary to realize the regime of strong heat exchange is given by:

$$\zeta = C_v\cdot\frac{A_{channel}}{A_{rad.area}}\cdot v_f = C_v\cdot\frac{d}{L}\cdot v_f \gg 4\sigma T_a^3 \quad \Rightarrow \quad v_f \gg \frac{4\sigma T_a^3}{C_v}\cdot\frac{L}{d} \sim 0.5\ \frac{mm}{s} \tag{25}$$

We note that thus found coolant speed is quite modest and can be easily realized via passive gravitationally driven liquid flow. Indeed, by mounting a radiative cooler of temperature T_c on top of a smart window of temperature T_w, due to coolant density dependence on temperature, this arrangement will produce a pressure differential across the window/cooler assembly:

$$\Delta P = \left(\rho(T_c) - \rho(T_w)\right) gL \sim \rho(T_a)\, gL\cdot\alpha_f\cdot(T_c - T_w) \tag{26}$$

where the cooler fluid thermal expansion coefficient is $\alpha_f \sim 2\cdot 10^{-4}$ (water), coolant density at the ambient temperature is $\rho(T_a) \sim 10^3\ kg/m^3$ (water), and a freefall acceleration is $g \approx 9.8\ m/s^2$. This pressure differential then drives an upward flow of the hot coolant from a smart window and a downward flow of the cold coolant from a radiative cooler. For the coolant flow confined to a narrow channel of size d, and assuming that the channel width is comparable to the channel length $\sim L$ one can then define the channel hydrolic resistance as $R_c = 12\frac{\mu}{d^3}$, where the coolant viscosity is $\mu \sim 10^{-3}[Pa\cdot s]$ (water). The hydrolic resistance can then be used to relate the pressure differential across the channel to the volume flow rate

through the channel $\partial V/\partial t \left[m^3/s\right]$, or equivalently to the gravitationally driven heat transfer rate (per unit area, per unit temperature) through the channel as follows:

$$\frac{\partial V}{\partial t}=\frac{\Delta P}{R_c} \quad \Rightarrow \quad \zeta_{grav}=\frac{C_v}{A_{rad.surface}}\frac{\partial V}{\partial t}=\frac{C_v}{A_{rad.surface}}\frac{\Delta P}{R_c}\sim\frac{\rho(T_a)C_v g\alpha_f}{12\mu}\cdot\frac{d^3}{L}\cdot(T_c-T_w) \quad (27)$$

Finally, in order to realize the strong heat exchange regime between a smart window and a radiative cooler using only gravitationally driven flow we must demand that:

$$\zeta_{grav}\gg 4\sigma T_a^3 \quad \Rightarrow \quad (T_c-T_w)\gg\frac{48\sigma T_a^3\mu}{\rho(T_a)C_v g\alpha_f}\frac{L}{d^3}\underset{water}{\sim}0.35\ K \quad (28)$$

As follows from Eq. (28) efficient heat exchange between a smart window and a radiative cooler is possible to realize by simply mounting one on top of the other and using a completely passive gravitationally driven flow, as long as temperature differential between the cooler and a window is larger than a fraction of one degree. Considering that standard radiative coolers can achieve temperatures that are tens of degrees below that of the ambient, then even under the daylight illumination conditions, we believe that proposed gravitationally driven heat exchange mechanism is viable.

SUMMARY

We have considered several simple physical models of the radiative coolers and partially transparent radiative windows. We have then distinguished the design goals for these two structures and provided optimal choice for the material parameters to realize these goals. Finally, we studied a thermally coupled window / radiative cooler system and showed how transmission of the visible light through the window can be enhanced without raising the window temperature above that of the ambient. Out findings can be summarized as follows:

Radiative cooling problem. Radiative coolers are normally non-transparent, and the main question is how to design a cooler so that the temperature on its dark side is as low as possible compared to that of the atmosphere. This is achieved when window is almost perfectly reflective in the visible $R_w^{VIS}\to 1$ (alternatively $T_w^{VIS}\to 0, A_w^{VIS}\to 0$), and when window absorption loss in the visible is much smaller than that in the mid-IR $A_w^{VIS}\ll\varepsilon_w^{MIR}$. Then, in the absence of convection, and for any choice of the material optical parameters in the mid-IR ($T_w^{MIR},\varepsilon_w^{MIR}$) $\min(T_w)=\min(T_s)=\varepsilon_a^{1/4}\cdot T_a\approx 0.94\cdot T_a$. In the presence of convection, radiative cooling efficiency reduces potentially to zero when convection is strong.

Partially transparent radiative window problem. For the radiative windows, their surfaces are partially transparent, and the main question is rather about the maximal visible light transmission through the window at which the temperature on the window somber side does not exceed that of the atmosphere. This is achieved when window transmission in the mid-IR is almost perfect $T_w^{MIR}\to 1$ (alternatively $R_w^{MIR}\to 0,\varepsilon_w^{MIR}\to 0$), while window absorption in the visible is small $A_w^{VIS}\to 0$ and at the same time much smaller than that in the mid-IR $A_w^{VIS}\ll\varepsilon_w^{MIR}$. Then, in the absence of convection, the maximal allowed transmission through the window in the visible is $T_w^{VIS}=\gamma=\frac{1-\varepsilon_a}{2-\varepsilon_a}=0.18$ while the wall, room and window temperatures are all smaller than the atmospheric one. If only requiring that the room and window temperatures are smaller than the atmospheric one, then the maximal transmission through the window in the visible can be increased to $T_w^{VIS}==\frac{4}{3}\gamma\approx 0.24$. In the presence of convection, maximal allowed window transmission in the visible reduces somewhat (at most as a certain multiplicative factor) even in the presence of strong convection.

Effect of convection. Convection contribution becomes important for high enough values of the heat transfer coefficient $h \gg 8\sigma T_a^3 (2T_w^{MIR} + \varepsilon_w^{MIR})$, which for the standard ambient temperatures is equivalent to $h \gg 12\left[W/\left(m^2 K\right)\right] \cdot (2T_w^{MIR} + \varepsilon_w^{MIR})$. The value of the heat transfer coefficient depends strongly on the temperature differential between the window and the ambient temperatures, as well as the window size and orientation and is generally in the $1-10\left[W/\left(m^2 K\right)\right]$ range for the non-forced convection (see Supplementary Material C for more details).

Finally, by thermally coupling smart windows to radiative coolers using passive or active flows of a fluid coolant placed inside of the window and cooler structures, one can significantly increase transmission of the visible light through the window, while keeping the window temperature below that of the ambient. This enhancement is a function of the heat transfer rate per unit temperature ζ, and the largest enhancement is achieved in the limit of strong heat exchange between a window and a cooler $\zeta \gg 4\sigma T_a^3 \sqrt{\varepsilon_w^{MIR} \varepsilon_c^{MIR}}$, which for the standard ambient temperatures is equivalent to $\zeta \gg 6\left[W/\left(m^2 K\right)\right] \sqrt{\varepsilon_w^{MIR} \varepsilon_c^{MIR}}$. Furthermore, strong heat exchange regime between radiative coolers and smart windows can be realized with small coolant velocities (sub *1mm/s* for ~*1m*-large windows) or even using a purely passive gravitationally driven coolant flows between a hot smart window and a cold radiative cooler mounted on top with minimal temperature differential (sub-*1K*) between the two.

ACKNOWLEDGMENT

We would like to acknowledge financial support of the l'Institut de l'énergie Trottier and Canada Research Chair of Prof. Skorobogatiy for this project.

REFERENCES

[1] Sorrell, S., 2015. “Reducing energy demand: A review of issues, challenges and approaches”. Renewable and Sustain-able Energy Reviews, 47, pp. 74–82.

[2] Kumar, A. R., Vijyakumar, K., and Sinivasan, P., 2014. “A review on passive cooling practices in residential buildings”. International Journal of Mathematical Sciences & Engineering (IJMSE), 3(1), pp. 1–5.

[3] Hossain, M. M., and Gu, M., 2016. “Radiative cooling: Principles, progress, and potentials”. Advanced Science, 3(7), p. 1500360.

[4] Catalanotti, S., Cuomo, V., Piro, G., Ruggi, D., Silvestrini, V., and Troise, G., 1975. “The radiative cooling of selective surfaces”. Solar Energy, 17(2), pp. 83–89.

[5] Zhao, B., Hu, M., Ao, X., Chen, N., and Pei, G., 2019. “Radiative cooling: A review of fundamentals, materials, applications, and prospects”. Applied Energy, 236, pp. 489–513.

[6] Santamouris, M., 2016. “Cooling the buildings–past, present and future”. Energy and Buildings, 128, pp. 617–638.

[7] Bahadori, M. N., 1978. “Passive cooling systems in iranian architecture”. Scientific American, 238(2), pp. 144–155.

[8] Granqvist, C., and Hjortsberg, A., 1981. “Radiative cooling to low temperatures: General considerations and applica-tion to selectively emitting sio films”. Journal of Applied Physics, 52(6), pp. 4205–4220.

[9] Berdahl, P., and Fromberg, R., 1982. “The thermal radiance of clear skies”. Solar Energy, 29(4), pp. 299–314.

[10] Suichi, T., Ishikawa, A., Hayashi, Y., and Tsuruta, K., 2018. “Performance limit of daytime radiative cooling in warm humid environment”. AIP Advances, 8(5), p. 055124.

[11] Long, S., Zhou, H., Bao, S., Xin, Y., Cao, X., and Jin, P., 2016. “Thermochromic multilayer films of wo 3/vo 2/wo 3 sandwich structure with enhanced luminous transmittance and durability”. RSC Advances, 6(108), pp. 106435–106442.

[12] DeForest, N., Shehabi, A., Garcia, G., Greenblatt, J., Masanet, E., Lee, E. S., Selkowitz, S., and Milliron, D. J., 2013. “Regional performance targets for transparent near-infrared switching electrochromic window glazings”. Building and Environment, 61, pp. 160–168.

[13] Raman, A. P., Anoma, M. A., Zhu, L., Rephaeli, E., and Fan, S., 2014. “Passive radiative cooling below ambient air temperature under direct sunlight”. Nature, 515(7528), p. 540.

[14] Tavares, P. F., Gaspar, A. R., Martins, A. G., and Frontini, F., 2014. “Evaluation of electrochromic windows impact in the energy performance of buildings in editerranean climates”. Energy Policy, 67, pp. 68–81.

[15] Runnerstrom, E. L., Llordés, A., Lounis, S. D., and Milliron, D. J., 2014. “Nanostructured electrochromic smart win-dows: traditional materials and nir-selective plasmonic nanocrystals”. Chemical communications, 50(73), pp. 10555–10572.

[16] Bamfield, P., 2010. Chromic phenomena: technological applications of colour chemistry. Royal Society of Chemistry.

[17] Rephaeli, E., Raman, A., and Fan, S., 2013. “Ultrabroadband photonic structures to achieve high-performance daytime radiative cooling”. Nano letters, 13(4), pp. 1457–1461.

[18] Mann, T. P., 2014. “Metamaterial window glass for adaptable energy efficiency”. PhD thesis.

[19] Shin, S., Hong, S., and Chen, R., 2018. “Hollow photonic structures of transparent conducting oxide with selective and tunable absorptance”. Applied Thermal Engineering, 145, pp. 416–422.

[20] Ye, H., Meng, X., Long, L., and Xu, B., 2013. “The route to a perfect window”. Renewable Energy, 55, pp. 448–455.

[21] Chen, Z., Zhu, L., Raman, A., and Fan, S., 2016. “Radiative cooling to deep sub-freezing temperatures through a 24-h day–night cycle”. Nature communications, 7, p. 13729.

[22] Berdahl, P., 1984. “Radiative cooling with mgo and/or lif layers”. Applied optics, 23(3), pp. 370–372.

[23] Gentle, A. R., and Smith, G. B., 2010. “Radiative heat pumping from the earth using surface phonon resonant nanopar-ticles”. Nano letters, 10(2), pp. 373–379.

[24] Yang, J., Xu, Z., Ye, H., Xu, X., Wu, X., and Wang, J., 2015. “Performance analyses of building energy on phase transition processes of vo2 windows with an improved model”. Applied energy, 159, pp. 502–508.

[25] Granqvist, C., 1990. “Chromogenic materials for transmittance control of large-area windows”. Critical Reviews in Solid State and Material Sciences, 16(5), pp. 291–308.

[26] Granqvist, C.-G., Green, S., Niklasson, G. A., Mlyuka, N. R., Von Kraemer, S., and Georén, P., 2010. “Advances in chromogenic materials and devices”. Thin Solid Films, 518(11), pp. 3046–3053.

[27] Granqvist, C.-G., Niklasson, G. A., and Azens, A., 2007. “Electrochromics: fundamentals and energy-related applica-tions of oxide-based devices”. Applied Physics A, 89(1), pp. 29–35.

[28] Long, L., and Ye, H., 2017. “Dual-intelligent windows regulating both solar and long-wave radiations dynamically”. Solar Energy Materials and Solar Cells, 169, pp. 145–150.

[29] Hillmer, H., Al-Qargholi, B., Khan, M. M., Worapattrakul, N., Wilke, H., Woidt, C., and Tatzel, A., 2018. “Optical mems-based micromirror arrays for active light steering in smart windows”. Japanese Journal of Applied Physics, 57(8S2), p. 08PA07.

[30] Korgel, B. A., 2013. “Materials science: composite for smarter windows”. Nature, 500(7462), p. 278.

[31] Llordés, A., Garcia, G., Gazquez, J., and Milliron, D. J., 2013. “Tunable near-infrared and visible-light transmittance in nanocrystal-in-glass composites”. Nature, 500(7462), p. 323.

[32] Long, L., and Ye, H., 2014. “How to be smart and energy efficient: A general discussion on thermochromic windows”. Scientific reports, 4, p. 6427.

[33] Ye, H., Meng, X., and Xu, B., 2012. “Theoretical discussions of perfect window, ideal near infrared solar spectrum regulating window and current thermochromic window”. Energy and Buildings, 49, pp. 164–172.

[34] Warwick, M. E., and Binions, R., 2014. “Advances in thermochromic vanadium dioxide films”. Journal of Materials Chemistry A, 2(10), pp. 3275–3292.

[35] Zhan, Y., Xiao, X., Lu, Y., Cao, Z., Qi, S., Huan, C., Ye, C., Cheng, H., Shi, J., Xu, X., et al., 2017. “The growth mechanism of vo2 multilayer thin films with high thermochromic performance prepared by rta in air”. Surfaces and Interfaces, 9, pp. 173–181.

[36] Liu, M., Su, B., Kaneti, Y. V., Chen, Z., Tang, Y., Yuan, Y., Gao, Y., Jiang, L., Jiang, X., and Yu, A., 2016. “Dual-phase transformation: Spontaneous self-template surface-patterning strategy for ultra-transparent vo2 solar modulating coatings”. ACS nano, 11(1), pp. 407–415.

[37] Zhu, B., Tao, H., and Zhao, X., 2016. “Effect of buffer layer on thermochromic performances of vo2 films fabricated by magnetron sputtering”. Infrared Physics & Technology, 75, pp. 22–25.

[38] Xu, F., Cao, X., Luo, H., and Jin, P., 2018. “Recent advances in vo 2-based thermochromic composites for smart windows”. Journal of Materials Chemistry C, 6(8), pp. 1903–1919.

[39] Zhang, J., He, H., Xie, Y., and Pan, B., 2013. “Theoretical study on the tungsten-induced reduction of transition temperature and the degradation of optical properties for vo2”. The Journal of chemical physics, 138(11), p. 114705.

[40] Lee, S. J., Choi, D. S., Kang, S. H., Yang, W. S., Nahm, S., Han, S. H., and Kim, T., 2019. “Vo2/wo3–based hybrid smart windows with thermochromic and electrochromic properties”. ACS Sustainable Chemistry & Engineering.

[41] Mandal, J., Du, S., Dontigny, M., Zaghib, K., Yu, N., and Yang, Y., 2018. “Li4ti5o12: A visible-to-infrared broadband electrochromic material for optical and thermal management”. Advanced Functional Materials, 28(36), p. 1802180.

[42] Dalapati, G. K., Kushwaha, A. K., Sharma, M., Suresh, V., Shannigrahi, S., Zhuk, S., and Masudy-Panah, S., 2018. “Transparent heat regulating (thr) materials and coatings for energy saving window applications: Impact of materials design, micro-structural, and interface quality on the thr performance”. Progress in materials science, 95, pp. 42–131.

[43] Berk, A., Conforti, P., Kennett, R., Perkins, T., Hawes, F., and Van Den Bosch, J., 2014. “Modtran 6: A major up-grade of the modtran radiative transfer code”. In 2014 6th Workshop on Hyperspectral Image and Signal Processing: Evolution in Remote Sensing (WHISPERS), IEEE, pp. 1–4.

[44] Howell, J. R., Menguc, M. P., and Siegel, R., 2015. Thermal radiation heat transfer. CRC press.

[45] Kusaka, H., Kondo, H., Kikegawa, Y., and Kimura, F., 2001. “A simple single-layer urban canopy model for atmospheric models: Comparison with multi-layer and slab models”. Boundary-layer meteorology, 101(3), pp. 329–358.

[46] Welty, J. R., Wicks, C. E., Rorrer, G., and Wilson, R. E., 2009. Fundamentals of momentum, heat, and mass transfer. John Wiley & Sons.

[47] Cengel, Y. A., Turner, R. H., and Cimbala, J. M., 2001. Fundamentals of thermal-fluid sciences, Vol. 703. McGraw-Hill New York.

[48] Goldstein, E.A., Raman, A.P., Fan, S., 2017. “Sub-ambient non-evaporative fluid cooling with the sky,” Nature Energy 2, 17143.

SUPPLEMENTARY MATERIAL A

Radiation heat transfer problem in 1D for a standalone slab with thermal conduction

Here we formulate radiative heat transfer equations in 1D for the case of a single plate irradiated with mid-IR radiation (see Fig. A1. (a)). We then solve the corresponding linearized version of the equations and show that in the limit of high enough thermal conductivity of the plate material, temperature inside of a plate can be considered constant. Furthermore, in this limit we also demonstrate that simple expressions for the radiative fluxes used throughout the paper can be derived from the full radiative heat transfer formulation.

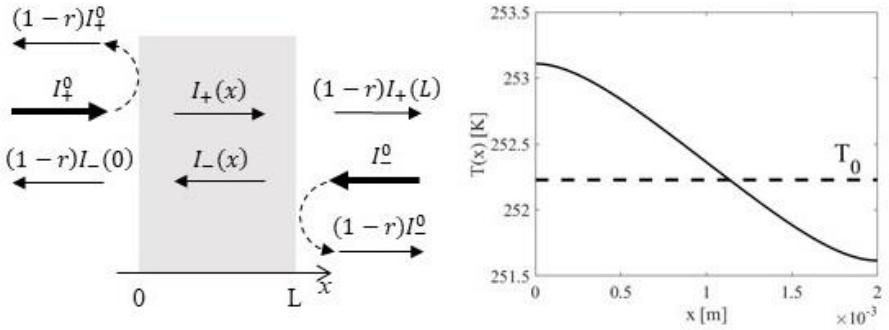

Fig A1. (Left) Schematic of an 1D radiative heat transfer problem. (Right) Typical temperature distribution across a thin plexiglass window.

Following Ref. 44, we define $I_+(x)$ to be the average mid-IR radiative flux propagating in the positive direction, $I_-(x)$ to be the average mid-IR radiative flux propagating in the negative direction, $T(x)$ to be the temperature distribution inside a plate, and $J(x)$ to be the heat flux due to thermal conduction. We consider that the plate is irradiated from the left by the mid-IR light with intensity I_+^0 and from the right by the mid-IR light with intensity I_-^0. Similar derivations can be performed when the plate is irradiated with the visible light, therefore we present only one derivation. We then define the plate material absorption loss in the mid-IR as α. The Fresnel reflection coefficient (by power) at the air/plate boundary is defined as $r=\left(\frac{n_m-n_a}{n_m+n_a}\right)^2$, where n_m, n_a are the material and air refractive indices in the mid-IR. A single pass transmission through the plate is defined as $t=\exp(-\alpha L)$, where L is the plate's thickness and $\alpha = 2\omega/c\cdot \mathrm{Im}(n_m)$. The plate's material thermal conductivity is defined as k. Finally, we assume that the plate's medium is non-scattering and that the local thermodynamic equilibrium approximation holds.

Taking into account material absorption of the mid-IR light, as well as thermal mid-IR re-emission, for the two radiative heat fluxes we can write:

$$\begin{aligned}\frac{\partial I_+(x)}{\partial x} &= -\alpha I_+(x)+\alpha\sigma T^4(x)\\ \frac{\partial I_-(x)}{\partial x} &= \alpha I_-(x)-\alpha\sigma T^4(x)\end{aligned} \qquad \text{(A.1)}$$

Furthermore, from the energy conservation and conductive thermal flux definition it follows that:

$$\begin{aligned}\alpha\left(I_+(x)+I_-(x)\right) &= 2\alpha\sigma T^4(x)+\frac{\partial J(x)}{\partial x}\\ J(x) &= -k\frac{\partial T(x)}{\partial x}\end{aligned} \qquad \text{(A.2)}$$

In the absence of heat transfer at the boundaries of a plate we use thermally isolating boundary conditions:

$$J(0) = J(L) = 0 \quad \text{(A.3)}$$

At the same time, incoming, forward and backward radiative fluxes are related through the optical boundary conditions at the interfaces expressed using Fresnel reflection coefficient r as follows:

$$\begin{aligned} I_+(0) &= rI_-(0) + (1-r)I_+^0 \\ I_-(L) &= rI_+(L) + (1-r)I_-^0 \end{aligned} \quad \text{(A.4)}$$

Equations (A.1-2) with boundary conditions (A.3-4) can be solved numerically. A typical temperature distribution across the plate is shown in Fig. A1 (b) for the case of a polycarbonate window $n_m = 1.5$, $r = 0.04$, $\alpha = 3200m^{-1}$, $L = 2mm$, $t = 0.017$, $k = 0.2W/(mK)$ and illumination intensity from the left $I_+^0 = 459\,W/m^2$ which corresponds to that of a black body at 300^0C (here we assume that $I_-^0 = 0$). From the figure we see that the temperature at the plate's illuminated side is somewhat higher than the temperature at the plate's somber side, while the overall temperature variation inside the is rather weak for this choice of the material's parameters.

In fact, if we assume that the temperature inside the plate varies weakly, $T(x) = T_0 + \Delta T(x)$, $\Delta T(x) << T_0$, then nonlinear temperature terms in equations (a.1-2) can be substituted with high precision by their corresponding linear approximation $T^4(x) \approx T_0^4 + 4T_0^3 \Delta T(x)$. In this case, linearized heat transfer problem (A.1-2) with boundary conditions (A.3-4) can be solved analytically, resulting in a purely exponential spatial dependence of the forward and backward propagating fluxes and temperature inside the plate. Moreover, the plate average temperature is simply related to the total incoming flux as $2\sigma T_0^4 = I_+^0 + I_-^0$, which is expected from the energy conservation.

Furthermore, assuming that heat conductivity of the plate material is high enough so that $k \gg 4\sigma T_0^3 L$ and at the same time $k \gg 8\sigma T_0^3/\alpha$, then the relative temperature differential across the plate is maximal when materials are strongly absorbing in the mid-IR $\alpha L \gg 1$, and equals to:

$$\frac{|T(L) - T(0)|}{T_0} \approx \frac{I_+^0 - I_-^0}{I_+^0 + I_-^0} \cdot \frac{\sigma T_0^3 L}{k}(1-r) < \frac{\sigma T_0^3 L}{k}(1-r)$$

Finally, in the same limit of high enough thermal conductivity of the plate material, the two outgoing mid-IR fluxes (to the left and to the right of the plate) are simply related to the incoming fluxes I_+^0, I_-^0 and the thermal flux radiated by the plate σT_0^4 via the plate net absorption A_p, reflection R_p and transmission T_p coefficients. These are exactly the classical expressions used throughout the paper:

total energy flux in the $+\infty$ direction, $x > L$:

$$(1-r)I_+(L) = R_p \cdot I_-^0 + T_p \cdot I_+^0 + A_p \cdot \sigma T_0^4$$

total energy flux in the $-\infty$ direction, $x < 0$:

$$rI_+^0 + (1-r)I_-(0) = R_p \cdot I_+^0 + T_p \cdot I_-^0 + A_p \cdot \sigma T_0^4$$

where the plate absorption A_p, reflection R_p and transmission T_p coefficients (by power) are given by the following expressions:

$$R_p = r + \frac{(1-r)^2 t^2 r}{1-r^2 t^2} = r[1+(1-r)^2 t^2 + (1-r)^2 r^2 t^4 + (1-r)^2 r^4 t^6]$$

$$T_p = t\frac{(1-r)^2}{1-r^2 t^2} = (1-r)^2 t(1+r^2 t^2 + \cdots)$$

$$A_p = \varepsilon_p = \frac{(1-t)(1-r)}{1-rt} = 1 - R_p - T_p$$

We also note that thus derived expressions for the plate reflection, absorption and transmission coefficients also correspond exactly to those that can be derived by assuming multiple ray passage through a thick absorbing optical medium after summing all the contribution of the partially transmitted, absorbed and reflected rays (see Fig A2).

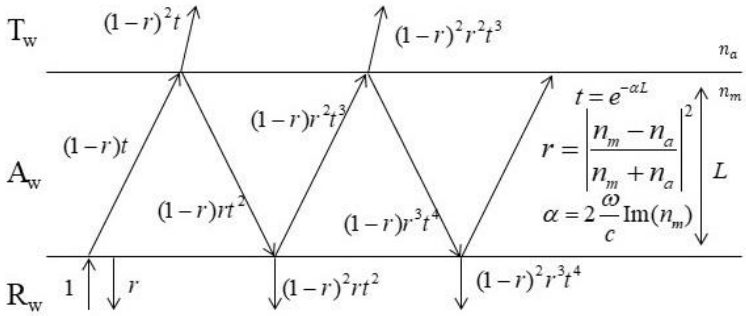

Fig A2. Transmission through and reflection from the optically thick plate (phase information is lost) can be described via addition of the energy fluxes of all the partially transmitted and reflected rays bouncing infinitely inside the plate.

Exact solution of the 1D linearized radiative heat transfer problem for a single slab

For completeness of the presentation, in what follows we present an exact solution of the 1D linearized radiative heat transfer problem (A.1-2) with boundary conditions (A.3-4). First, we define the following dimensionless parameters:

$$\tilde{I}_+(\tilde{x}) = \frac{I_+(x)}{\langle I \rangle} - 1 \quad ; \quad \tilde{I}_-(\tilde{x}) = \frac{I_-(x)}{\langle I \rangle} - 1$$

$$\tilde{T}(\tilde{x}) = \frac{T(x)}{T_0} - 1 \quad ; \quad \tilde{J}(\tilde{x}) = \frac{J(x)}{\langle I \rangle}$$

$$\tilde{x} = \alpha x \quad ; \quad \langle I \rangle = \sigma T_0^4 \quad ; \quad \eta = \frac{\sigma T_0^3}{\alpha k} \quad ; \quad \lambda = \sqrt{1+8\eta}$$

Then, assuming weak variation of the temperature across the plate $T(x) = T_0 + \Delta T(x)$, $\Delta T(x) << T_0$, we substitute the nonlinear temperature terms in equations (A.1-2) with the corresponding linear approximation $T^4(x) \approx T_0^4 + 4T_0^3 \Delta T(x)$. This allows us to rewrite the original nonlinear equations (A.1-2) in the following linear form:

$$\frac{\partial \tilde{I}_+(\tilde{x})}{\partial \tilde{x}} = -\tilde{I}_+(\tilde{x}) + 4\tilde{T}(\tilde{x})$$
$$\frac{\partial \tilde{I}_-(\tilde{x})}{\partial \tilde{x}} = \tilde{I}_-(\tilde{x}) - 4\tilde{T}(\tilde{x})$$
$$\frac{\partial \tilde{J}(\tilde{x})}{\partial \tilde{x}} = \tilde{I}_+(\tilde{x}) + \tilde{I}_-(\tilde{x}) - 8\tilde{T}(\tilde{x})$$
$$\frac{\partial \tilde{T}(\tilde{x})}{\partial \tilde{x}} = -\eta \tilde{J}(\tilde{x})$$

The corresponding boundary conditions are:

$$\tilde{T}(0) = -\tilde{T}(\alpha L)$$
$$\tilde{J}(0) = \tilde{J}(\alpha L) = 0$$
$$\tilde{I}_+(0) = r\tilde{I}_-(0) + (1-r)\left(\frac{I_+^0}{\langle I \rangle} - 1\right)$$
$$\tilde{I}_-(\alpha L) = r\tilde{I}_+(\alpha L) + (1-r)\left(\frac{I_-^0}{\langle I \rangle} - 1\right)$$

One can then show that the following expression is an analytical solution of the linearized radiative heat transfer problem that satisfies the abovementioned boundary conditions:

$$\begin{pmatrix} \tilde{I}_+(\tilde{x}) \\ \tilde{I}_-(\tilde{x}) \\ \tilde{J}(\tilde{x}) \\ \tilde{T}(\tilde{x}) \end{pmatrix} = C\left(-\frac{\alpha L}{2}\begin{pmatrix} 4 \\ 4 \\ 0 \\ 1 \end{pmatrix} + \begin{pmatrix} 4\tilde{x}-4 \\ 4\tilde{x}+4 \\ -1/\eta \\ \tilde{x} \end{pmatrix} + \frac{1}{\lambda\eta}\begin{pmatrix} \frac{4\eta}{1+\lambda} \\ \frac{4\eta}{1-\lambda} \\ -\lambda \\ \eta \end{pmatrix} \frac{e^{\lambda\tilde{x}} - e^{-\lambda(\alpha L - \tilde{x})}}{e^{-\lambda\alpha L} - e^{\lambda\alpha L}} + \frac{1}{\lambda\eta}\begin{pmatrix} \frac{4\eta}{1-\lambda} \\ \frac{4\eta}{1+\lambda} \\ \lambda \\ \eta \end{pmatrix} \frac{e^{-\lambda\tilde{x}} - e^{\lambda(\alpha L - \tilde{x})}}{e^{-\lambda\alpha L} - e^{\lambda\alpha L}} \right)$$

where, in addition, $\langle I \rangle = \frac{I_+^0 + I_-^0}{2}$, $\Delta I = I_+^0 - I_-^0$ and:

$$C = -\frac{\Delta I}{4\langle I \rangle} \cdot \left(\alpha L + \left(2 + \frac{1}{4\eta}\right)\left(\frac{1+r}{1-r}\right) + \frac{1}{4\lambda\eta}\frac{1-e^{-\lambda\alpha L}}{1+e^{-\lambda\alpha L}} \right)^{-1}.$$

Finally, the relative temperature drop across the plate is given by the following expression:

$$\frac{T(L) - T(0)}{T_0} = -\frac{\Delta I}{4\langle I \rangle} \cdot \frac{\alpha L - \frac{2}{\lambda}\frac{1-e^{-\lambda\alpha L}}{1+e^{-\lambda\alpha L}}}{\alpha L + \left(2 + \frac{1}{4\eta}\right)\left(\frac{1+r}{1-r}\right) + \frac{1}{4\lambda\eta}\frac{1-e^{-\lambda\alpha L}}{1+e^{-\lambda\alpha L}}}.$$

SUPPLEMENTARY MATERIAL B

Effect of convection on the thermal properties of a single layer optically symmetric window

In this model we add convection heat transfer between window and air that surrounds it, while ignoring heat conduction through the air. The model is virtually identical to the model without convection (Section 3), with only two new parameters, which are the room temperature (T_r, space between the window and the wall), and the heat transfer coefficient h. Value of the heat transfer coefficient is in general temperature dependent and can be significantly different for horizontal or vertical surfaces. In Supplementary Material C, for completeness, we present several well-known models for the heat transfer coefficient at the planar interfaces between gas and solid.

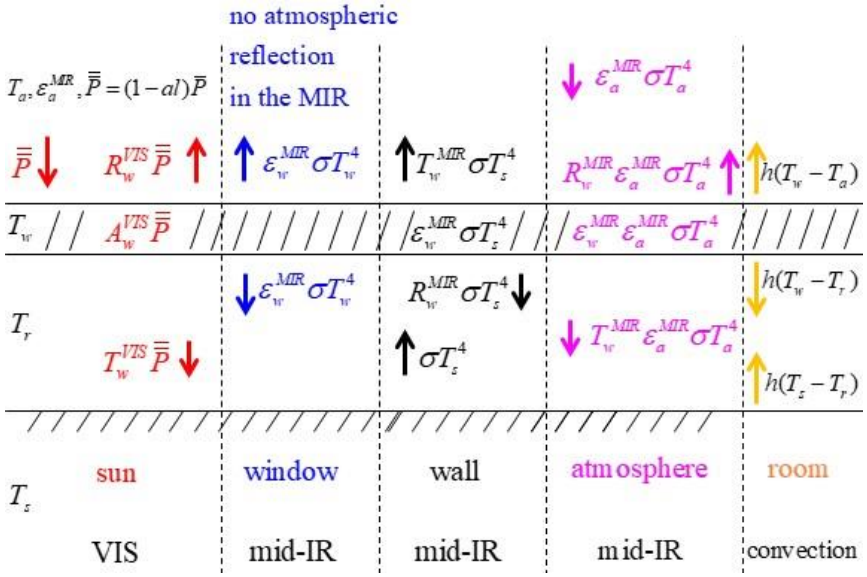

Fig. B1. Model of the optically symmetric single layer window (with convection)

We now use the energy conservation principle to write the following equations (see Fig. B1). At the window / atmosphere interface we write for the energy fluxes in equilibrium:

$$\int (1-r_w(\nu))\cdot P_g(\nu)\,d\nu = \int \varepsilon_w(\nu)\cdot E(\nu,T_w)\,d\nu + \int t_w(\nu)\cdot E(\nu,T_s)\,d\nu - \int (1-r_w(\nu))\cdot \varepsilon_a(\nu)\cdot E(\nu,T_a)\,d\nu + h(T_w-T_a) \quad \text{(B.1)}$$

At the window / room interface we write for the energy fluxes in equilibrium:

$$\int t_w(\nu)\cdot P_g(\nu)\,d\nu = -\int \varepsilon_w(\nu)\cdot E(\nu,T_w)\,d\nu + \int (1-r_w(\nu))\cdot E(\nu,T_s)\,d\nu - \int t_w(\nu)\cdot \varepsilon_a(\nu)\cdot E(\nu,T_a)\,d\nu - h(T_w-T_r) \quad \text{(B.2)}$$

By subtracting (B.2) from (B.1) we also get the balance between the absorbed and irradiated energy in the window, as well as heat transferred into the window due to convection:

$$2\int \varepsilon_w(\nu)\cdot E(\nu,T_w)\,d\nu = \int \alpha_w(\nu)\cdot P(\nu)\,d\nu + \int \alpha_w(\nu)\cdot E(\nu,T_s)\,d\nu + \int \alpha_w(\nu)\cdot \varepsilon_a(\nu)\cdot E(\nu,T_a)\,d\nu + h(2T_w-T_a-T_r) \quad \text{(B.3)}$$

Finally, in thermal equilibrium, two convection flows inside of the room have to cancel each other:

$$h(T_s-T_r)+h(T_w-T_r)=0 \Rightarrow T_r=\frac{T_s+T_w}{2} \quad \text{(B.4)}$$

Assuming step-like spectral properties of the window material optical properties in (B.1-B.3) (see Fig. 4) we can then write the following system of equations (only 2 of them are independent):

$$\begin{cases} (1-R_w^{VIS})\cdot \bar{\bar{P}} = \varepsilon_w^{MIR}\cdot\sigma T_w^4 + T_w^{MIR}\cdot\sigma T_s^4 - (1-R_w^{MIR})\cdot\varepsilon_a\sigma T_a^4 + h(T_w-T_a) \\ T_w^{VIS}\cdot\bar{\bar{P}} = -\varepsilon_w^{MIR}\cdot\sigma T_w^4 + (1-R_w^{MIR})\cdot\sigma T_s^4 - T_w^{MIR}\cdot\varepsilon_a\sigma T_a^4 - h(T_w-T_r) \\ 2\varepsilon_w^{MIR}\cdot\sigma T_w^4 = A_w^{VIS}\cdot\bar{\bar{P}} + \varepsilon_w^{MIR}\cdot\sigma T_s^4 + \varepsilon_w^{MIR}\cdot\varepsilon_a\sigma T_a^4 + h(T_w-T_a) + h(T_w-T_r) \end{cases} \quad \text{(B.5)}$$

Now, using results of a single layer model of the atmosphere that relates atmospheric temperature to the average light power arriving at the planet surface, we can arrive to the following coupled nonlinear equations for the temperatures of the window and the wall:

$$\frac{T_w^4}{T_a^4}+\frac{h}{\sigma T_a^3(2T_w^{MIR}+\varepsilon_w^{MIR})}\left(\frac{T_w-T_a}{T_a}+\frac{3T_w-T_s-2T_a}{2T_a}\frac{T_w^{MIR}}{\varepsilon_w^{MIR}}\right)=\varepsilon_a+\left(2-\varepsilon_a\right)\frac{T_w^{VIS}+A_w^{VIS}\cdot\left(1+\frac{T_w^{MIR}}{\varepsilon_w^{MIR}}\right)}{2T_w^{MIR}+\varepsilon_w^{MIR}}$$

$$\frac{T_s^4}{T_a^4}+\frac{h}{\sigma T_a^3(2T_w^{MIR}+\varepsilon_w^{MIR})}\left(\frac{T_w+T_s-2T_a}{2T_a}\right)=\varepsilon_a+\left(2-\varepsilon_a\right)\frac{2T_w^{VIS}+A_w^{VIS}}{2T_w^{MIR}+\varepsilon_w^{MIR}} \qquad \text{(B.6)}$$

These equations can be solved analytically by linearizing the nonlinear terms assuming that the wall and window temperatures are close to the atmospheric temperature $\frac{T_{s,w}^4}{T_a^4}\approx 1+4\frac{\delta T_{s,w}}{T_a}$, where $\delta T_{s,w}=T_{s,w}-T_a$. In this case, a system of nonlinear equations (B.6) becomes linear:

$$4\frac{\delta T_w}{T_a}+\underbrace{\frac{h}{2\sigma T_a^3(2T_w^{MIR}+\varepsilon_w^{MIR})}}_{\chi}\left(\frac{\delta T_w}{T_a}\left(2+3\frac{T_w^{MIR}}{\varepsilon_w^{MIR}}\right)-\frac{\delta T_s}{T_a}\frac{T_w^{MIR}}{\varepsilon_w^{MIR}}\right)=\underbrace{\left(\varepsilon_a-1\right)+\left(2-\varepsilon_a\right)\frac{T_w^{VIS}+A_w^{VIS}\cdot\left(1+\frac{T_w^{MIR}}{\varepsilon_w^{MIR}}\right)}{2T_w^{MIR}+\varepsilon_w^{MIR}}}_{X_w}$$

$$4\frac{\delta T_s}{T_a}+\underbrace{\frac{h}{2\sigma T_a^3(2T_w^{MIR}+\varepsilon_w^{MIR})}}_{\chi}\left(\frac{\delta T_w}{T_a}+\frac{\delta T_s}{T_a}\right)=\underbrace{\left(\varepsilon_a-1\right)+\left(2-\varepsilon_a\right)\frac{2T_w^{VIS}+A_w^{VIS}}{2T_w^{MIR}+\varepsilon_w^{MIR}}}_{X_s} \qquad \text{(B.7)}$$

and can be solved analytically to give the following expressions:

$$\frac{\delta T_w}{T_a}=\frac{4X_w+\chi\left(X_w+X_s\frac{T_w^{MIR}}{\varepsilon_w^{MIR}}\right)}{(4+\chi)(4+\chi(2+3\frac{T_w^{MIR}}{\varepsilon_w^{MIR}}))+\chi^2\frac{T_w^{MIR}}{\varepsilon_w^{MIR}}}$$

$$\frac{\delta T_s}{T_a}=\frac{4X_s+\chi\left(X_s(2+3\frac{T_w^{MIR}}{\varepsilon_w^{MIR}})-X_w\right)}{(4+\chi)(4+\chi(2+3\frac{T_w^{MIR}}{\varepsilon_w^{MIR}}))+\chi^2\frac{T_w^{MIR}}{\varepsilon_w^{MIR}}} \qquad \text{(B.8)}$$

$$\frac{\delta T_r}{T_a}=\frac{\delta T_s+\delta T_w}{2T_a}=\frac{2X_w+2X_s+\chi X_s(1+2\frac{T_w^{MIR}}{\varepsilon_w^{MIR}})}{(4+\chi)(4+\chi(2+3\frac{T_w^{MIR}}{\varepsilon_w^{MIR}}))+\chi^2\frac{T_w^{MIR}}{\varepsilon_w^{MIR}}}$$

Analysis of thermal properties of a single layer radiative window with convection

1) A particular solution of Eq. (B.6) for which convection terms do not contribute is $T_w=T_s=T_w$ when choosing $T_w^{VIS}=\gamma\cdot T_w^{MIR}$, $A_w^{VIS}=\gamma\cdot\varepsilon_w^{MIR}$, for any values of $T_w^{MIR},\varepsilon_w^{MIR}$ and h.

2) We now study how addition of convection influences maximal allowed transmission of the visible light T_w^{VIS} through the window. As a design condition we demand that either the window temperature or

the wall temperature or the room temperature do not exceed the atmospheric one $T_{w,s,r} < T_a$. From (B.8), without making any assumption on the strength of a convection coefficient we find that the abovementioned design conditions define the following allowed regions in the T_w^{VIS}, A_w^{VIS} parameter space (equations in blue in (B.9)):

$$\text{Window temperature: } \delta T_w < 0 \Rightarrow 4X_w + \chi\left(X_w + X_s \frac{T_w^{MIR}}{\varepsilon_w^{MIR}}\right) < 0$$

$$\left(1+\frac{\chi}{4}\left(1+2\frac{T_w^{MIR}}{\varepsilon_w^{MIR}}\right)\right)\cdot T_w^{VIS} + \left(1+\frac{T_w^{MIR}}{\varepsilon_w^{MIR}}+\frac{\chi}{4}\left(1+2\frac{T_w^{MIR}}{\varepsilon_w^{MIR}}\right)\right)\cdot A_w^{VIS} < 2\gamma\left(T_w^{MIR}+\frac{\varepsilon_w^{MIR}}{2}\right)\left(1+\frac{\chi}{4}\left(1+\frac{T_w^{MIR}}{\varepsilon_w^{MIR}}\right)\right)$$

$$\max\left(T_w^{VIS}\right)_{A^{VIS}=0} = 2\gamma\left(T_w^{MIR}+\frac{\varepsilon_w^{MIR}}{2}\right)\cdot f_w(\chi) < 2\gamma\left(T_w^{MIR}+\frac{\varepsilon_w^{MIR}}{2}\right) \quad \forall\chi$$

$$\text{where } f_w(\chi) = \frac{1+\frac{\chi}{4}\left(1+\frac{T_w^{MIR}}{\varepsilon_w^{MIR}}\right)}{1+\frac{\chi}{4}\left(1+2\frac{T_w^{MIR}}{\varepsilon_w^{MIR}}\right)} \to \begin{cases} 1, \chi \to 0 \text{ - weak convection} \\ \dfrac{1+\frac{T_w^{MIR}}{\varepsilon_w^{MIR}}}{1+2\frac{T_w^{MIR}}{\varepsilon_w^{MIR}}} \in \left(\frac{1}{2},1\right), \chi \to \infty \text{ - strong convection} \end{cases}$$

$$\text{Wall temperature: } \delta T_s < 0 \Rightarrow 4X_s + \chi\left(X_s(2+3\frac{T_w^{MIR}}{\varepsilon_w^{MIR}}) - X_w\right) < 0$$

$$\left(2+\frac{3\chi}{4}\left(1+2\frac{T_w^{MIR}}{\varepsilon_w^{MIR}}\right)\right)\cdot T_w^{VIS} + \left(1+\frac{\chi}{4}\left(1+2\frac{T_w^{MIR}}{\varepsilon_w^{MIR}}\right)\right)\cdot A_w^{VIS} < 2\gamma\left(T^{MIR}+\frac{\varepsilon^{MIR}}{2}\right)\left(1+\frac{\chi}{4}\left(1+3\frac{T_w^{MIR}}{\varepsilon_w^{MIR}}\right)\right)$$

$$\max\left(T_w^{VIS}\right)_{A^{VIS}=0} = \gamma\left(T_w^{MIR}+\frac{\varepsilon_w^{MIR}}{2}\right)\cdot f_s(\chi) < \gamma\left(T_w^{MIR}+\frac{\varepsilon_w^{MIR}}{2}\right) \quad \forall\chi \qquad \text{(B.9)}$$

$$\text{where } f_s(\chi) = \frac{1+\frac{\chi}{4}\left(1+3\frac{T_w^{MIR}}{\varepsilon_w^{MIR}}\right)}{1+\frac{3\chi}{8}\left(1+2\frac{T_w^{MIR}}{\varepsilon_w^{MIR}}\right)} \to \begin{cases} 1, \chi \to 0 \text{ - weak convection} \\ \dfrac{\frac{2}{3}+2\frac{T_w^{MIR}}{\varepsilon_w^{MIR}}}{1+2\frac{T_w^{MIR}}{\varepsilon_w^{MIR}}} \in \left(\frac{2}{3},1\right), \chi \to \infty \text{ - strong convection} \end{cases}$$

$$\text{Room temperature: } \delta T_r < 0 \Rightarrow 2X_w + 2X_s + \chi X_s(1+2\frac{T^{MIR}}{\varepsilon^{MIR}}) < 0$$

$$\left(3+\chi\left(1+2\frac{T^{MIR}}{\varepsilon^{MIR}}\right)\right)\cdot T^{VIS} + \left(2+\frac{T^{MIR}}{\varepsilon^{MIR}}+\frac{\chi}{2}\left(1+2\frac{T^{MIR}}{\varepsilon^{MIR}}\right)\right)\cdot A^{VIS} < 4\gamma\left(T^{MIR}+\frac{\varepsilon^{MIR}}{2}\right)\left(1+\frac{\chi}{4}\left(1+2\frac{T^{MIR}}{\varepsilon^{MIR}}\right)\right)$$

$$\max\left(T_w^{VIS}\right)_{A^{VIS}=0} = \frac{4}{3}\gamma\left(T^{MIR}+\frac{\varepsilon^{MIR}}{2}\right)\cdot f_r(\chi) < \frac{4}{3}\gamma\left(T^{MIR}+\frac{\varepsilon^{MIR}}{2}\right) \quad \forall\chi$$

$$\text{where } f_r(\chi) = \frac{1+\frac{\chi}{4}\left(1+2\frac{T^{MIR}}{\varepsilon^{MIR}}\right)}{1+\frac{\chi}{3}\left(1+2\frac{T^{MIR}}{\varepsilon^{MIR}}\right)} \to \begin{cases} 1, \chi \to 0 \text{ - weak convection} \\ \frac{3}{4}, \chi \to \infty \text{ - strong convection} \end{cases}$$

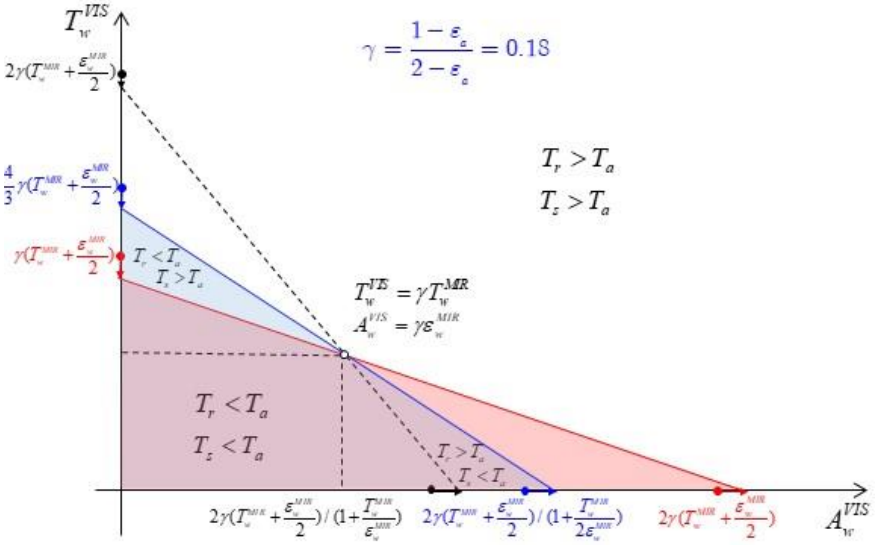

Fig. B2. Tradeoff between window transmission and absorption in the visible (with convection). A region of parameter space which is situated below the two lines define window operation regime for which both the wall and the room temperatures are smaller than that of the atmosphere. For completeness, a third dotted line is presented along which the window temperature is equal to that of the atmosphere.

Tradeoff between window transmission and absorption in the visible can be summarized geometrically in Fig. B2. As follows from inequalities presented in (B.9), regions below the corresponding lines represent the range of values of T_w^{VIS}, A_w^{VIS} for which either the window temperature or the wall temperature or the room temperature are smaller than the atmospheric one. For practical purposes, we are mostly interested in the room temperature and the wall temperature (shaded regions in Fig. B2). Intersection of the corresponding two regions represent the range of values of T_w^{VIS}, A_w^{VIS} for which both the wall temperature and the room temperature are smaller than the atmospheric one. Both the window, the wall and the room temperatures attain that of the atmospheric one when $T_w^{VIS} = \gamma \cdot T_w^{MIR}$, $A_w^{VIS} = \gamma \cdot \varepsilon_w^{MIR}$. As clear from the graph, when $T_w^{VIS} \le \gamma \cdot T_w^{MIR}$ and $A_w^{VIS} \le \gamma \cdot \varepsilon_w^{MIR}$, it is guaranteed that both the window and the room temperatures will be smaller than the atmospheric temperature. Also, from (B.9) we observe that the maximal allowed value of the transmitted light in the visible reduces somewhat when convection is present. The new value represents a fraction of the original value when no convection is present.

3) We now study how addition of convection influences minimal achievable values of the window, wall and room temperatures in the problem of radiative cooling. Particularly, as follows from the single layer model of a window (without convection), radiative cooling is most efficient when window is almost perfectly reflective in the visible, and when window absorption loss in the visible is much smaller than that in the mid-IR, which can be summarized as $T_w^{VIS} \to 0, A_w^{VIS} \to 0, A_w^{VIS} \ll \varepsilon_w^{MIR}$. In the absence of convection, we then found that $\min\left(T_w\right) = \min\left(T_s\right) = \min\left(T_r\right) = \varepsilon_a^{1/4} \cdot T_a \approx 0.94 \cdot T_a$, or alternatively $\min\left(\frac{\delta T_w}{T_a}\right) = \min\left(\frac{\delta T_s}{T_a}\right) = \min\left(\frac{\delta T_r}{T_a}\right) \approx \frac{\varepsilon_a - 1}{4} = 0.055$. When convection is present, from analysis of the linearized equations (B.8) it follows that for the radiative cooling to be most efficient, the same conditions as in the case without convection have to be satisfied $T_w^{VIS} \to 0, A_w^{VIS} \to 0, A_w^{VIS} \ll \varepsilon_w^{MIR}$. In this case, $X_s = X_w = \varepsilon_a - 1$ and from the following expressions for the minimal achievable window, wall, and room temperatures we conclude that the cooling efficiency degrades (minimal achievable temperatures grow):

$$\left.\begin{aligned}
\min\left(\frac{\delta T_w}{T_a}\right) &= \frac{(\varepsilon_a - 1)}{4}\cdot\frac{1+\frac{\chi}{4}\left(1+\frac{T_w^{MIR}}{\varepsilon_w^{MIR}}\right)}{\left(1+\frac{\chi}{4}\right)\left(1+\frac{\chi}{4}\left(2+3\frac{T_w^{MIR}}{\varepsilon_w^{MIR}}\right)\right)+\left(\frac{\chi}{4}\right)^2\frac{T_w^{MIR}}{\varepsilon_w^{MIR}}} \\
\min\left(\frac{\delta T_s}{T_a}\right) &= \frac{(\varepsilon_a - 1)}{4}\frac{1+\frac{\chi}{4}\left(1+3\frac{T_w^{MIR}}{\varepsilon_w^{MIR}}\right)}{\left(1+\frac{\chi}{4}\right)\left(1+\frac{\chi}{4}\left(2+3\frac{T_w^{MIR}}{\varepsilon_w^{MIR}}\right)\right)+\left(\frac{\chi}{4}\right)^2\frac{T_w^{MIR}}{\varepsilon_w^{MIR}}} \\
\min\left(\frac{\delta T_r}{T_a}\right) &= \frac{(\varepsilon_a - 1)}{4}\frac{1+\frac{\chi}{4}\left(1+2\frac{T_w^{MIR}}{\varepsilon_w^{MIR}}\right)}{\left(1+\frac{\chi}{4}\right)\left(1+\frac{\chi}{4}\left(2+3\frac{T_w^{MIR}}{\varepsilon_w^{MIR}}\right)\right)+\left(\frac{\chi}{4}\right)^2\frac{T_w^{MIR}}{\varepsilon_w^{MIR}}}
\end{aligned}\right\} = \frac{(\varepsilon_a - 1)}{4}\cdot\begin{cases} 1, \chi \to 0, \text{weak convection} \\ \sim\frac{1}{\chi}, \chi \to \infty, \text{strong convection} \end{cases} \quad \text{(B.10)}$$

SUPPLEMENTARY MATERIAL C

Models for the temperature dependent heat transfer coefficients at the planar gas/solid interfaces are well known and can be found for example in [46]. In what follows we present expressions that assume laminar flows along either horizontal or vertical interfaces. For both orientations a key parameter is a Rayleigh number [47] that can be expressed as follows:

$$Ra_L = \frac{g\beta}{\nu\alpha}(T_s - T_\infty)L^3,$$

where $\beta = \frac{1}{T_f}$ is the expansion coefficient for ideal gases, ν is the kinematic viscosity, α is the thermal diffusivity and L is the ratio of the plate surface area to its perimeters, k is heat conductivity of air, $g = 9.8\left[m/s^2\right]$ is the free fall acceleration. As the gas properties are temperature dependent, they are evaluated at the so-called film temperature $T_f = (T_s + T_\infty)/2$, which is the average of the surface T_s and the surrounding bulk temperature T_∞. The following are expressions for the various parameters of air:

$$\nu(T_f) = \mu(T_f)/\rho(T_f),$$

where dynamic viscosity

$$\mu(T_f) = 2.55628\times10^{-7}\times T_f^{0.741}\ \left[Pa\cdot s\right]$$

$$k(T_f) = k_0 T_f^{0.8755} = 1.7254\times10^{-4}\times T_f^{0.8755}\ \left[W/(m\cdot K)\right]$$

$$\rho(T_f) = \frac{P_{atm}}{R\cdot T_f} = \frac{352.97}{T_f}\left[\frac{kg}{m^3}\right] \quad ; \quad C_p = \frac{7}{2}R \approx 1005\frac{J}{kg\cdot K} \quad ; \quad \alpha(T_f) = \frac{k(T_f)}{\rho(T_f)C_p}$$

Then, for the Ryleigh number at the solid/air interface we find:

$$Ra = \frac{C_P\cdot\frac{1}{T_f}\cdot\left(\frac{P_{atm}}{R\cdot T_f}\right)^2 g}{k_0\cdot\mu_0\cdot T_f^{0.74}\cdot T_f^{0.88}} \approx \frac{g\cdot\frac{7}{2}P_{atm}^2}{R\cdot k_0\cdot\mu_0}\times\frac{1}{T_f^{4.6174}} \approx \frac{2.7769\times10^{19}}{T_f^{4.6174}}(T_s - T_\infty)L^3.$$

Heat transfer coefficient for the horizontal plate (Laminar flow)

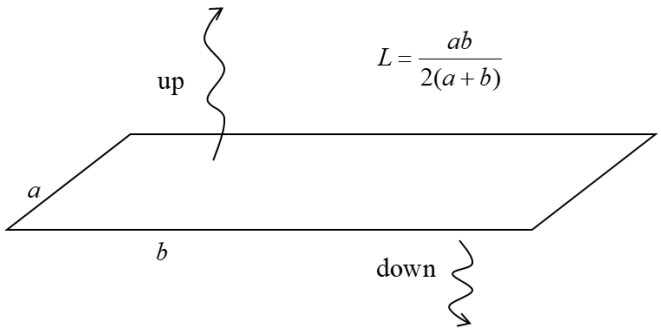

Fig C1. Heat transfer coefficient for the horizontal plate (Laminar flow)

Hot surface facing up (or cold facing down),

$$h_{horisontal} = \frac{k}{L}\cdot 0.54\cdot Ra_L^{\frac{1}{4}}, \qquad 10^5 < Ra_L < 2\times10^7$$

As hot air is moving up and cold air is moving down, convection heat transfer is more efficient for hot surfaces facing up or cold surfaces facing down.

Alternatively, for the hot surface facing down (or cold facing up)

$$h_{horisontal} = \frac{k}{L} \cdot 0.27 \cdot Ra_L^{\frac{1}{4}}$$

Thus, for the two cases we get the following expressions for the heat transfer coefficients:

$$h = \begin{pmatrix} 2 \\ 1 \end{pmatrix} \cdot 3.33815 \cdot \left(\frac{T_s - T_\infty}{L \cdot T_f} \right)^{\frac{1}{4}} \cdot \frac{1}{T_f^{0.0289}}$$

Heat transfer coefficient for the vertical plate (Laminar flow)

$$h_{horisontal} = \frac{k}{L}\left(0.68 + \frac{0.67}{\left(1 + \left(\frac{0.492}{\Pr}\right)^{\frac{9}{16}}\right)^{\frac{4}{9}}} \cdot Ra_L^{\frac{1}{4}}\right)$$

where the Pratt number for air is defined as:

$$\Pr = \frac{\nu}{\alpha} = \frac{\mu C_p}{k} = \frac{7}{2} R \frac{\mu_0 T_f^{0.74}}{k_0 T_f^{0.88}} \approx \frac{7}{2} \frac{R}{T_f^{0.1336}} \frac{\mu_0}{k_0} \approx \frac{1.4924}{T_f^{0.1336}}$$

Thus, leading to the following approximative expression for the heat transfer coefficient at the air/solid interface (inclined at an angle θ with respect to the vertical ($\theta \in (0, 60^\circ)$):

$$h = \frac{1.1733 \times 10^{-4}}{L} T_f^{0.8755} + 6.4273 \left(\frac{T_s - T_\infty}{L T_f} \right)^{\frac{1}{4}} \frac{(\cos\theta)^{\frac{1}{4}}}{T_f^{0.0289}}$$

At $T_f \approx 300K$, the first term on the right hand in the expression is normally small (for example it equals to 0.017 when $L = 1m$, and it equals to 0.17 when $L = 0.1m$). The second term is normally much larger (it equals to 2.73 when $L = 1m$ and $T_s - T_\infty = 1^o C$, and it equals to 4.86 when $L = 0.1m$ and $T_s - T_\infty = 10^o C$).